

Mechanisms of Regional Winter Sea-Ice Variability in a Warming Arctic

JAKOB DÖRR,^a MARIUS ÅRTHUN,^a TOR ELDEVIK,^a AND ERICA MADONNA^a

^a *Geophysical Institute, University of Bergen, and Bjerknes Centre for Climate Research, Bergen, Norway*

(Manuscript received 18 February 2021, in final form 21 July 2021)

ABSTRACT: The Arctic winter sea ice cover is in retreat overlaid by large internal variability. Changes to sea ice are driven by exchange of heat, momentum, and freshwater within and between the ocean and the atmosphere. Using a combination of observations and output from the Community Earth System Model Large Ensemble, we analyze and contrast present and future drivers of the regional winter sea ice cover. Consistent with observations and previous studies, we find that for the recent decades ocean heat transport through the Barents Sea and Bering Strait is a major source of sea ice variability in the Atlantic and Pacific sectors of the Arctic, respectively. Future projections show a gradually expanding footprint of Pacific and Atlantic inflows highlighting the importance of future Atlantification and Pacification of the Arctic Ocean. While the dominant hemispheric modes of winter atmospheric circulation are only weakly connected to the sea ice, we find distinct local atmospheric circulation patterns associated with present and future regional sea ice variability in the Atlantic and Pacific sectors, consistent with heat and moisture transport from lower latitudes. Even if the total freshwater input from rivers is projected to increase substantially, its influence on simulated sea ice is small in the context of internal variability.

SIGNIFICANCE STATEMENT: The winter sea ice cover in the Arctic is declining due to global warming, but the decline is quite variable because of the chaotic nature of the climate system. We want to understand what causes this variability, both for the present and the next decades, and for different regions of the Arctic. We find that now and in the future, variability in the winter sea ice is influenced by transport of oceanic heat and atmospheric heat and moisture from the Pacific and Atlantic side of the Arctic. These findings improve our understanding of what influences changes in the winter sea ice cover, and could help to improve predictions of sea ice in the Arctic.


KEYWORDS: Arctic; Sea ice; Atmospheric circulation; Climate models; Climate variability; Interannual variability; Internal variability


1. Introduction

Over the last decades, the sea ice in the Arctic has significantly declined in all seasons (Notz and Stroeve 2016; Onarheim et al. 2018). The loss of Arctic sea ice potentially impacts Arctic Ocean hydrography (Polyakov et al. 2020) and atmospheric circulation outside the Arctic (Vihma 2014; Cohen et al. 2020). Climate models project a continued loss of Arctic sea ice in the next few decades as a result of global warming, and the summer sea ice is expected to disappear sometime before the middle of this century (Notz and SIMIP Community 2020; Årthun et al. 2021). This externally forced loss of sea ice is overlaid by substantial internal variability on all time scales (Ding et al. 2019; England et al. 2019), which can mask human-induced trends (Swart et al. 2015) and is the dominant source of uncertainty in projections of Arctic sea ice in the coming decades (Bonan et al. 2021). Understanding the

drivers and mechanisms underlying internal climate variability in the Arctic can thus enhance the ability to predict interannual to decadal variations in sea ice cover. Here we focus on sea ice variability in winter, which is expected to become more pronounced in the future Arctic (Onarheim et al. 2018; Årthun et al. 2021).

The potential drivers of sea ice variability assessed in this study include ocean heat transport (OHT) into the Arctic Ocean, large-scale atmospheric circulation, and river runoff. Ocean heat transport has been one of the largest drivers of recent winter sea ice variability (Francis and Hunter 2007; Carmack et al. 2015; Årthun et al. 2019). Most oceanic heat enters the Arctic Ocean through three different gateways (Fig. 1). Warm Atlantic Water enters the Eurasian Basin in two branches, one via the Fram Strait (Rudels et al. 2015) and one through the Barents Sea Opening (BSO) via the Barents and Kara Seas (Schauer et al. 2002). The heat transported by these branches impacts the sea ice north of Svalbard and in the Barents Sea (Sandø et al. 2010; Schlichtholz 2011; Årthun et al. 2012; Lind and Ingvaldsen 2012; Onarheim et al. 2014; Lien et al. 2017). Farther into the Arctic, the Atlantic Water is separated from the surface by the Arctic halocline (Aagaard et al. 1981), but

 Denotes content that is immediately available upon publication as open access.

 Supplemental information related to this paper is available at the Journals Online website: <https://doi.org/10.1175/JCLI-D-21-0149.s1>.

Corresponding author: Jakob Dörr, jakob.dorr@uib.no

DOI: 10.1175/JCLI-D-21-0149.1

© 2021 American Meteorological Society



This article is licensed under a Creative Commons Attribution 4.0 license (<http://creativecommons.org/licenses/by/4.0/>).

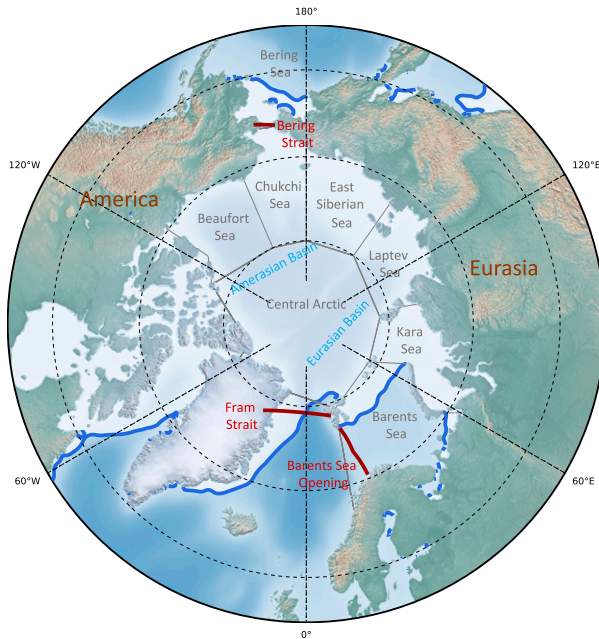


FIG. 1. Map of the Arctic Ocean showing the regional seas (gray), main oceanic basins (light blue), and oceanic gateways (red) used in this work. White shading with the blue contour shows the average observed winter (November–March) sea ice edge (50% sea ice concentration) between 1990 and 2019.

observations suggest a recent weakening of this halocline and a subsequent increase in the Atlantic Water influence on the surface layers and the sea ice in the Eurasian Basin (Polyakov et al. 2017, 2018). The increasing influence of Atlantic Water within the Arctic is commonly referred to as an Atlantification of the Arctic Ocean (Årthun et al. 2012; Polyakov et al. 2017). On the other side of the Arctic, Pacific surface water enters the Arctic Ocean through the 50-m-deep Bering Strait (Woodgate 2018). The Bering Strait OHT influences the water temperatures and sea ice cover in the Chukchi Sea (Woodgate et al. 2012; Serreze et al. 2016). Although it is well established that OHT influences the Arctic sea ice cover, the different footprints of the main inflow branches on winter sea ice and how these are expected to evolve in the future have not been compared and assessed.

Atmospheric variability in winter influences the sea ice cover through thermodynamic and dynamic mechanisms. The thermodynamic mechanisms alter the surface energy fluxes, notably through advection of heat and moisture from lower latitudes (e.g., Woods and Caballero 2016; Olonscheck et al. 2019; Gimeno et al. 2019; Nygård et al. 2020). This advection causes local warming through enhanced cloud cover and increased sensible and latent heat fluxes and downwelling radiation, which slows sea ice growth (Hegyí and Taylor 2017). This effect is enhanced by local feedback in open water created by sea ice loss (Kim et al. 2019; Rehder et al. 2020). The dynamic mechanisms include the motion and export of sea ice due to winds (e.g., Cai et al. 2020). The spatial patterns of thermodynamic and dynamic mechanisms have been related to

large-scale modes of winter atmospheric circulation (Deser et al. 2000; Rigor et al. 2002; Zhang et al. 2003; Luo et al. 2017; Cai et al. 2020). For example, sea ice loss in the Barents–Kara Seas has been shown to be connected to enhanced heat and moisture transport occurring during episodes of Ural blocking during the positive phase of the North Atlantic Oscillation (Luo et al. 2017; Gong and Luo 2017; Zhong et al. 2018). Similarly, sea ice variability in the Bering and Chukchi Seas has been found to be connected to atmospheric blocking over Alaska and atmospheric moisture transport over the Pacific (Woods and Caballero 2016; Blackport et al. 2019). While the atmospheric circulation patterns most connected to regional sea ice variability are well established for the recent past using reanalysis and models, it has not been studied in detail how these patterns might change in the future under a strongly reduced winter sea ice cover, and especially whether large-scale hemispheric modes such as the Arctic Oscillation might see an increased connection to the regional sea ice.

The river runoff into the Arctic Ocean potentially influences the sea ice either directly through heat input or indirectly through freshwater input, which alters the stratification of the upper ocean. Park et al. (2020) found the river input in early summer to increase sea ice melt and subsequent atmospheric and oceanic temperatures, which could impact the sea ice in winter. On the other hand, increased river runoff acts to increase stratification that separates the sea ice from the warmer Atlantic-origin waters below (Carmack et al. 2016), which would lead to increased sea ice growth in winter (Nummelin et al. 2016). It remains unclear, however, whether variable river runoff is important for the internal variability of winter sea ice in a fully coupled system.

Because the mechanisms governing internal variability in the winter Arctic sea ice cover differ between regions in the Arctic Ocean (Francis and Hunter 2007), it is important to assess the drivers for different regions separately. Furthermore, as the future winter sea ice loss expands to more regions of the Arctic Ocean (Årthun et al. 2021), the relative importance of the mechanisms influencing variability might change (Holland and Stroeve 2011). In this study, we assess the main oceanic and atmospheric drivers of internal winter Arctic sea ice variability for different regions in the Arctic Ocean, and investigate how these drivers will change in the future. Such a regional and temporal comparison of both oceanic and atmospheric drivers in the fully coupled system presents the main novelty of our study. To assess the different drivers of winter sea ice variability, we use a combination of observations and simulations from the Community Earth System Model Large Ensemble (CESM-LE; Kay et al. 2015), which has been widely used and extensively evaluated for Arctic sea ice variability (Barnhart et al. 2016; Jahn et al. 2016; England et al. 2019; Desmarais and Tremblay 2021), ocean heat transport (Auclair and Tremblay 2018; Årthun et al. 2019), and atmospheric circulation variability (Wettstein and Deser 2014; Ding et al. 2017; Wang et al. 2019a).

The paper is structured as follows. Data and methods are presented in section 2. In section 3, we analyze and compare the observed and simulated mean state, variability, and future

evolution of the winter sea ice and the oceanic and atmospheric drivers. We then analyze the connection of oceanic heat transport, atmospheric circulation, and river runoff to winter sea ice in sections 4, 5, and 6, respectively. Although our main focus is on interannual variability, we also assess internally driven trends for different time scales in section 7. The results are discussed and summarized in section 8.

2. Data and methods

a. CESM-LE

We use the output from 40 members of the Community Earth System Model's Large Ensemble (CESM-LE; Kay et al. 2015) from 1990 to 2080, which are forced by the historical (1920–2005) and RCP8.5 (2006–2100) forcing scenarios. We note that RCP8.5 is a high-emission (worst case) scenario, and that its use in near-term predictions is debated (Hausfather and Peters 2020). Other emission scenarios are, however, not assessed here. All members are subject to the same external forcing but differ in their initial conditions, such that differences between the simulations arise solely due to internal variability simulated by the model. We analyze three distinct periods: 1990–2019, representing the recent past, 2020–49, representing a near-future period, and 2050–79, representing a far-future period.

We investigate winter sea ice, defined as November to March of the following year. We analyze both the mean sea ice concentration (using the model variable AICE), as well as the total pan-Arctic and regional sea ice area, which is calculated as the area of a grid cell times its sea ice concentration, summed up over all grid cells in the target region, and using the native land mask of the source data. We calculate the sea ice area for all regions shown in Fig. 1, using the regional mask provided by the National Snow and Ice Data Center (NSIDC; available online from <ftp://sidacs.colorado.edu/DATASETS/NOAA/G02186/ancillary/>).

We calculate the ocean heat transport through the three main gateways to the Arctic Ocean: The Fram Strait, the Barents Sea Opening (BSO), and the Bering Strait (Fig. 1). The ocean heat transport (OHT) through a section S is defined as follows:

$$\text{OHT} = \rho c_p \int_S \mathbf{U}(T - T_{\text{ref}}) dS, \quad (1)$$

where $\rho = 1025 \text{ kg m}^{-3}$ is the constant water density, $c_p = 4000 \text{ J K}^{-1} \text{ kg}^{-1}$ is the constant heat capacity of the ocean, \mathbf{U} is the velocity normal to the section, T is the temperature, and S is the surface area of the section. In the CESM, we calculate OHT directly from the advective heat flux (model variables UET and VNT). As we calculate the OHT through individual nonclosed sections, it will depend on a somewhat arbitrary reference temperature T_{ref} . In CESM, a reference temperature of 0°C is used for the advective heat flux. For the Bering Strait and the BSO, we calculate the net poleward heat transport, while for the Fram Strait we consider the heat transport associated with the northward flow only (i.e., the Atlantic inflow by the West Spitsbergen Current) in order not to include the southward flowing East Greenland Current in the calculation. The influence of BSO OHT on the Barents Sea sea ice is largest

when OHT lags around 1–2 years (e.g., Årthun et al. 2012), while the influence of Bering Strait OHT mainly originates from the summer and autumn months (Serreze et al. 2016) when the Bering Strait is ice-free and the heat transport is largest (see Fig. S1 in the online supplemental material). To enable consistent averaging periods between available observations and CESM for all three gateways, we thus choose to relate the annual mean OHT from January to December to the following winter sea ice. Changing the averaging period for OHT in CESM-LE to the same winter instead leads similar patterns for BSO and Fram Strait, but weaker patterns for Bering Strait OHT, since its annual maximum is not captured (not shown).

We calculate the total annual river runoff in the CESM from the model variable QCHOCNR. Because we focus on the central Arctic, we only sum up the runoff from the following regions: the Canadian Archipelago, Beaufort Sea, Bering Sea, Chukchi Sea, East Siberian Sea, Laptev Sea, and Kara Sea. From these regional time series, we define the North American runoff as the sum over the first three regions, and Russian runoff as the sum over the latter four regions. For Arctic river runoff, CESM-LE compares well to observational estimates (Jahn and Laiho 2020).

Furthermore, to investigate the relationship of atmospheric circulation variability with winter sea ice variability we analyze the monthly mean sea level pressure (model variable PSL) and surface winds (variables UBOT and VBOT). To capture the two leading modes of winter atmospheric circulation, we apply principal component analysis to the area-weighted winter mean sea level pressure anomalies field north of 20°N .

For all analysis beyond the overview in chapter 3, we isolate internal variability by subtracting the ensemble mean from each ensemble member, thereby removing the forced trend resulting from the increase in greenhouse gas concentrations. To assess connections between the interannual variability of sea ice and its potential drivers, we calculate anomaly correlations and regressions for the different periods by concatenating the time series over a period from all 40 members, obtaining a time series of 40×30 years. To assess internally driven sea ice trends, we perform ensemble trend correlations over the ensemble dimension (40 members). For all regressions and correlations with sea ice area or concentration, we multiply the indices by -1 , so that the coefficients correspond to a decrease in sea ice.

b. Observations

We use observations and reanalysis products to analyze the drivers of sea ice variability during recent decades (1990–2019) and to evaluate the CESM-LE's ability to reproduce these drivers.

We use monthly sea ice concentration derived from satellite observations and provided by the EUMETSAT Ocean and Sea Ice Satellite Application Facility (OSI SAF; Lavergne et al. 2019) to calculate the total Arctic sea ice area, as well as the sea ice areas for the regions analyzed in this work. Furthermore, we use observational estimates of the annual mean ocean heat transports obtained through long-term mooring records in the Bering Strait (1999–2015; Woodgate 2018), the BSO (1998–2016; Ingvaldsen et al. 2004), and Fram Strait (West

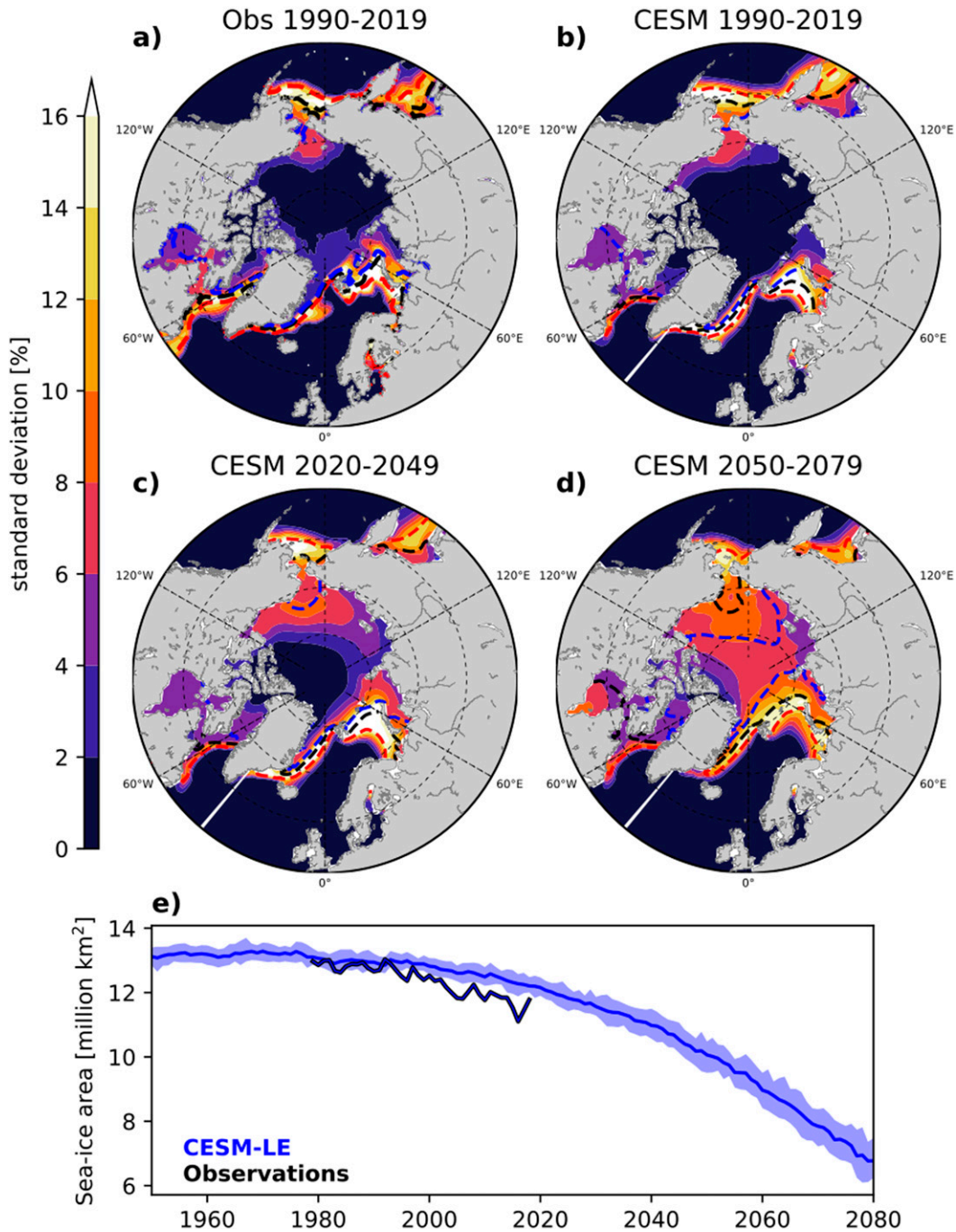


FIG. 2. Observed and simulated Arctic winter sea ice cover. (a)–(d) Maps showing the standard deviation of the winter (November–March) sea ice concentration for (a) 1990–2019 in observations (OSI SAF) and (b)–(d) three periods in CESM-LE. Red, black, and blue show mean sea ice concentration of 15%, 50%, and 75%, respectively. (e) Time series of total Arctic winter sea ice area in CESM-LE and observations.

Spitsbergen Current) (1998–2011; [Beszczynska-Möller et al. 2012](#)). Although the time series of the observed heat transports are short and there are some inherent limitations with the data (like the spatial coverage of the mooring instruments), they provide a valuable tool for qualitatively comparing results from the CESM-LE for the present period. Unlike CESM-LE, which

uses a reference temperature of 0°C, the reference temperature used for the observed Bering Strait heat transport is -1.9°C . To enable a rough comparison with the estimate from the CESM-LE, we follow [Auclair and Tremblay \(2018\)](#) and estimate the resulting difference in heat transport by multiplying the average observed annual mean volume transport of 0.96 Sv

($1 \text{ Sv} \equiv 10^6 \text{ m}^3 \text{ s}^{-1}$) with the reference temperature difference and subtract the resulting 7.5 TW from the observed values.

Observation-based estimates of atmospheric variability (monthly mean sea level pressure and surface winds) are obtained from the ERA5 (Hersbach et al. 2020) between 1990 and 2019. We note that ERA5, like other reanalysis products, has a significant warm bias in winter surface temperatures over sea ice compared to observations (Graham et al. 2019).

To assess links between the observed ocean heat transport and atmospheric circulation variability and interannual sea ice variability, we calculate anomaly correlations from linearly detrended data.

3. Mean state, variability, and future change

We first evaluate to what extent CESM-LE is consistent with observations in its simulated mean state and variability of winter Arctic sea ice concentration, as well as in its representation of the drivers of variability that will be assessed in this study. We also evaluate the future changes in sea ice concentration and its potential drivers as projected by CESM-LE.

a. Sea ice concentration

For the recent decades, observations show that the variability in winter sea ice concentration has predominately occurred in the Barents Sea, the Bering Sea, and the Sea of Okhotsk (Fig. 2a). The observed decrease in the total winter sea ice area (Fig. 2e) mainly originates from those regions. The CESM-LE generally simulates a mean winter sea ice cover similar to observations (Fig. 2b), except for the Barents Sea where there is an excessive sea ice cover related to lower simulated ocean temperatures than observed (Park et al. 2014). Consequently, the CESM-LE overestimates the total Arctic winter sea ice area compared with observations (Fig. 2e). The CESM-LE also simulates less sea ice variability in Baffin Bay.

For future periods, the CESM-LE projects a continued strong variability in the Barents and Bering Seas, as well as an increased variability within the central Arctic Ocean (Figs. 2c,d). This coincides with a corresponding decrease in the ensemble mean sea ice concentration that also spreads poleward from the Atlantic and Pacific side. During 2050–79, most of the Arctic Ocean, except for the central basin and the Laptev Sea, has a mean winter sea ice concentration lower than 75% (Fig. 3), as the freeze-up is delayed into early winter. By then, the sea ice loss and variability increases in the whole Arctic Ocean, except for the southernmost shelf seas where the sea ice loss is more advanced (Figs. 3a,e).

b. Ocean heat transport

The Arctic sea ice cover—both its mean state and variability—is influenced by ocean heat transport (Carmack et al. 2015). Of the three main oceanic gateways to the Arctic Ocean, ocean heat transport is largest through the BSO, with a mean observational estimate of around 50 TW over 1990–2019 (Fig. 4a). The annual mean heat transport through the Bering Strait is estimated at 6 TW, and the Fram Strait heat transport at 23 TW. None of the observed heat transport time series show significant trends.

The CESM-LE is consistent with observations for the BSO heat transport, both for the mean and the variability, but underestimates the Bering Strait (4 TW) and the Fram Strait (10 TW) heat transport. We note, however, that for the BSO OHT, the observations do not include the contribution of the Norwegian Coastal Current, and that the estimate of total BSO OHT is closer to 70 TW (Smedsrud et al. 2013). The CESM-LE thus likely also underestimates the mean BSO OHT, which is consistent with the positive bias in sea ice area in the Barents Sea. For all three gateways, the CESM-LE projects a strong future increase in the ensemble mean heat transports. The strongest increase is in the Fram Strait, where the heat transport increases by around 30 TW by 2080. The increase in the Bering Strait and BSO is roughly 5 and 26 TW by 2080, respectively. In all three gateways, the increase in heat transport mainly stems from an increase in the inflow temperature (not shown).

c. Atmospheric circulation

The winter sea ice is also influenced by the winter atmospheric circulation (e.g., Zhang et al. 2003). We compare the two leading modes of winter sea level pressure in the observation-based reanalysis (ERA5) and the CESM-LE model in Figs. 4c–f. The pattern of the first mode represents the Arctic Oscillation (AO; Thompson and Wallace 1998), and the second mode is reminiscent of the Pacific–North American pattern (hereafter referred to as PNA*; Wallace and Gutzler 1981; Quadrelli and Wallace 2004; Overland and Wang 2005). The two leading modes are similar in ERA5 and CESM-LE, although in CESM-LE the AO is more dominant in the Pacific sector with a weaker Azores high, a bias common to Earth system models (Gong et al. 2016). For the PNA* pattern, there are large differences over Eurasia and the Barents–Kara Seas, although the dominant region over the North Pacific is similar. Note that, by construction, the principal component time series (i.e., the AO and PNA* indices) do not show any long-term trends.

d. River runoff

The input of heat and freshwater to the Arctic Ocean by river runoff is another potentially important source of sea ice variability (Nummelin et al. 2016; Park et al. 2020), as it is fundamental to maintaining a low-salinity Arctic surface layer susceptible to freezing (Nummelin et al. 2016). The CESM-LE simulates around 0.12 Sv of river runoff into the Arctic Ocean over the period 1990–2019 (Fig. 4b). About 60% of that originates from the Eurasian continent and about 40% from the American continent. The ensemble-mean runoff increases by around 25% by the year 2080, with a similar increase in both continents. This forced increase is similar to the 30% increase projected by the CMIP5 multimodel mean (Nummelin et al. 2016).

4. The role of ocean heat transport in winter sea ice variability

We now analyze the influence of annual mean OHT on the following winter (November–March) sea ice concentration for the three gateways: the BSO, Fram Strait, and Bering Strait. The choice of annual mean OHT corresponds to a lagged response

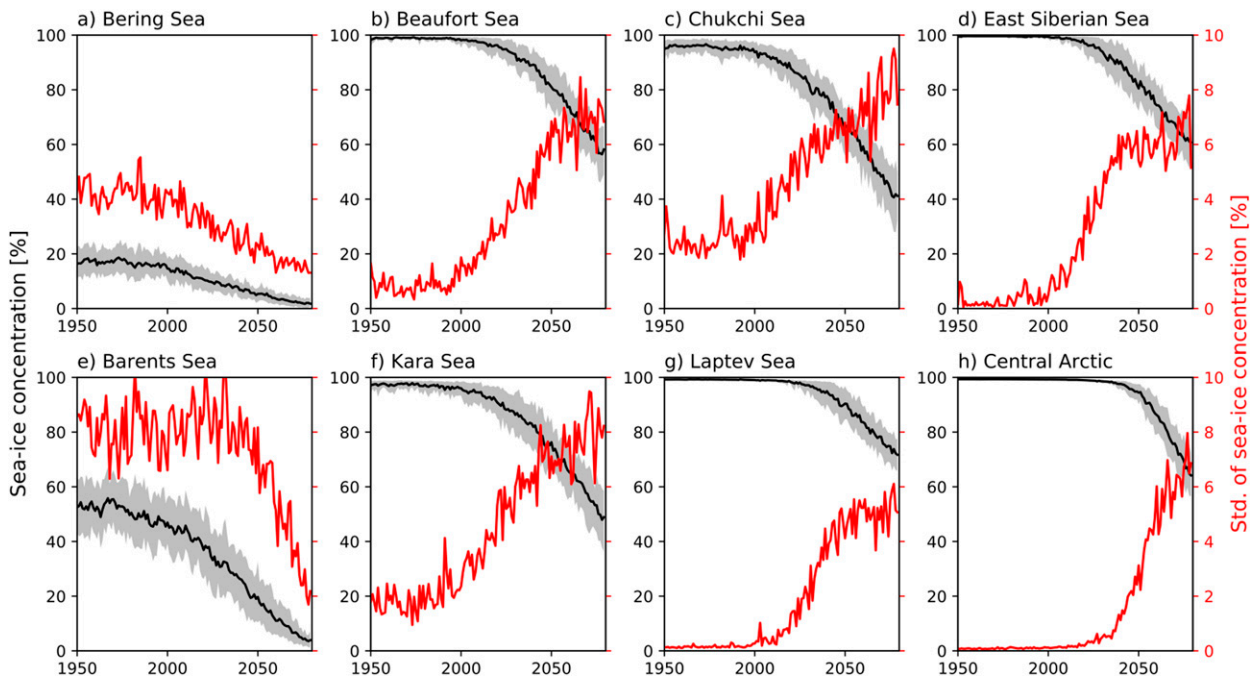


FIG. 3. Time series of ensemble mean (black line) winter (November–March) sea ice concentration, its interdecile range across cross members (gray shading), and its ensemble standard deviation (red) in eight different regions of the Arctic Ocean for the CESM-LE.

in winter sea ice of about 6 months. Increasing or decreasing this lag by a couple of months does not qualitatively change our results. We compare the influence in CESM-LE to available observations over the last decades and proceed to analyze changes in the influence in two future periods in the CESM-LE.

a. Barents Sea Opening

Available observations from the recent decades reveal there is no significant influence of the BSO heat transport on the winter sea ice in the Barents Sea (Fig. 5a), although we reiterate that the observational record is short. Previous studies did however find an influence of observed ocean heat transport on winter sea ice area when the heat transport leads by 1–2 years (e.g., [Årthun et al. 2012](#); [Onarheim et al. 2015](#)). For CESM-LE, there is a clear relationship between BSO heat transport and winter sea ice concentration in the Barents Sea over the period 1990–2019, considering both the following winter (Fig. 5b, positive correlations) and subsequent winter (not shown). Positive anomalies in BSO heat transport are associated with reduced sea ice concentration in the entire Barents Sea, as well as in the adjacent Kara and Greenland Seas. For future periods, the CESM-LE projects a continued but weakening influence of BSO heat transport on sea ice in the Barents Sea (Figs. 5c,d). The impact is also seen to expand eastward toward the Kara and Laptev Seas, roughly along the pathway of Atlantic waters entering the Arctic Ocean (e.g., [Rudels et al. 2015](#)).

Considering the correlation between OHT and different regional sea ice areas (Fig. 6), we find that the BSO heat transport has the largest influence in the Barents and Kara Seas (Fig. 6a), and that the influence expands toward the Laptev Sea in the future. The total Arctic sea ice area (rightmost column in Fig. 6) is most

strongly impacted by the BSO heat transport in the first two periods, as most variability in the winter Arctic sea ice is located in the Barents Sea (Figs. 2a,b), but this influence weakens in the future.

To further understand the influence of the BSO heat transport, we assess in Figs. 7a–c its influence on water temperatures along vertical sections that follow the approximate inflow pathway. A stronger BSO heat transport is associated with higher temperatures in the entire water column throughout the Barents Sea and into the St. Anna Trough (around 70°E) for all three periods (Figs. 7a–c, positive correlations). This is consistent with Atlantic-origin water covering the whole water column in the northeastern Barents Sea in winter ([Schauer et al. 2002](#)). Beyond the Barents Sea, the BSO heat transport is negatively correlated with temperatures just below the surface mixed layer during 1990–2019, which is consistent with weaker stratification and deeper winter mixed layers in the eastern Eurasian Basin during years of enhanced Atlantic Water transport ([Polyakov et al. 2017](#)). In the future periods, this negative correlation weakens and eventually disappears, likely because the direct effect of warmer Atlantic Water inflow becomes more important. Additionally, anomalous temperatures in the upper 100-m spread from the Barents Sea into the eastern Eurasian Basin. This suggests that Atlantic-origin waters from the Barents Sea are able to reach the mixed layer in the eastern Eurasian Basin in winter, and is corroborated by a positive correlation of the annual mean BSO heat transport with the mixed layer salinity in this area (not shown).

b. Fram Strait

The change in sea ice concentration associated with Fram Strait heat transport is similar to that for the BSO heat transport,

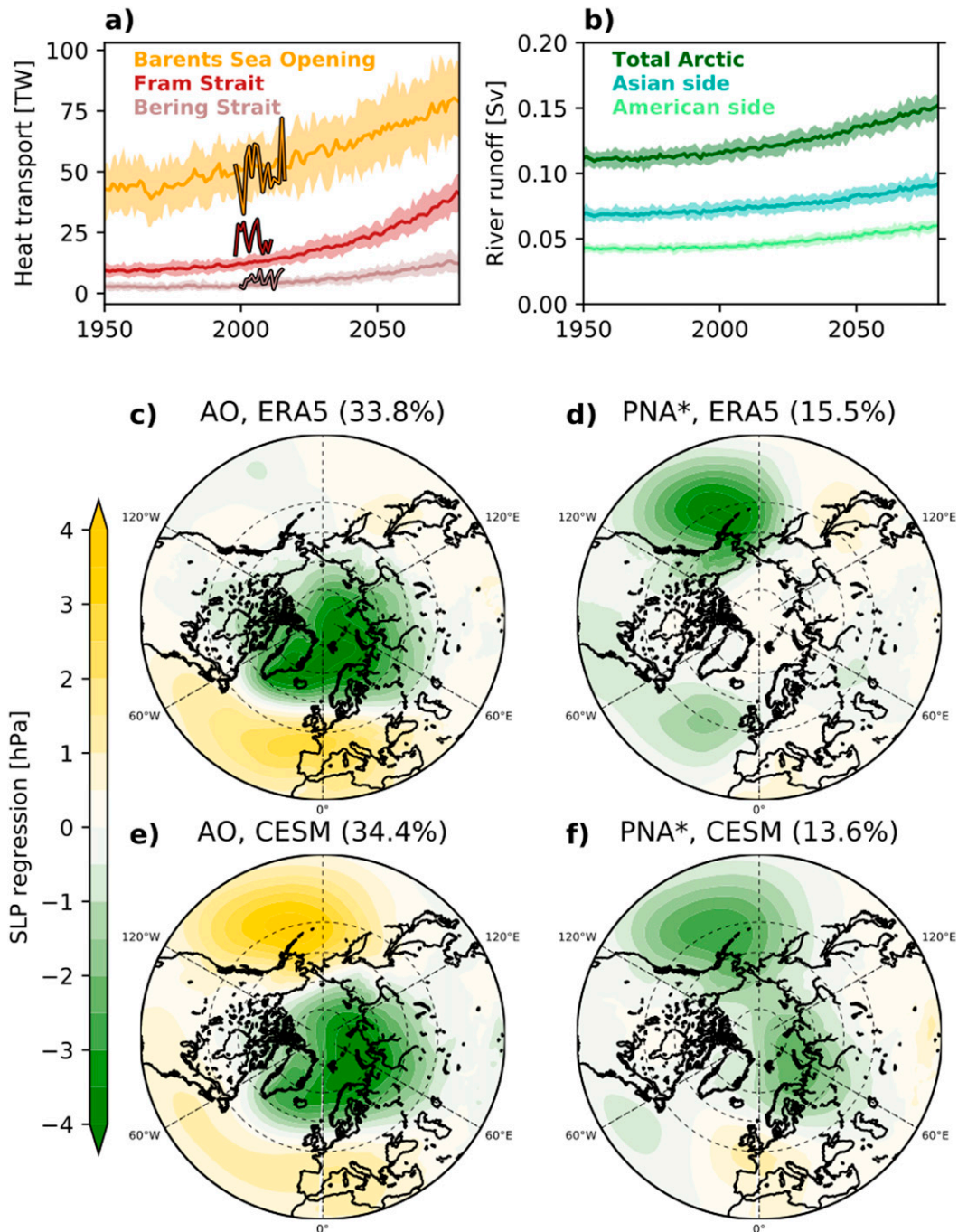


FIG. 4. Time series of (a) annual mean ocean heat transport through the Fram Strait, BSO, and Bering Strait in CESM-LE and observations (thick lines) and (b) annual mean river runoff in CESM-LE. Shading shows interdecile range of ensemble members in CESM-LE. Also shown are regressions of winter mean sea level pressure onto the principal components of the first two leading modes in (c),(d) ERA5 and (e),(f) CESM-LE, the Arctic Oscillation (AO), and the Pacific–North America–like (PNA*) patterns. Fraction of explained variance is given in parentheses.

both for observations and the CESM-LE (Figs. 5e,f). The influence of the Fram Strait heat transport on the sea ice weakens in future periods (Figs. 5g,h), but, unlike the BSO heat transport, does not show any spatial progression. The influence on the

regional sea ice areas remains limited to the Barents and Greenland Seas (Fig. 6b). This limited influence on downstream sea ice can be understood by looking at the influence on ocean temperature (Figs. 7d–f), which is mainly confined to the deeper

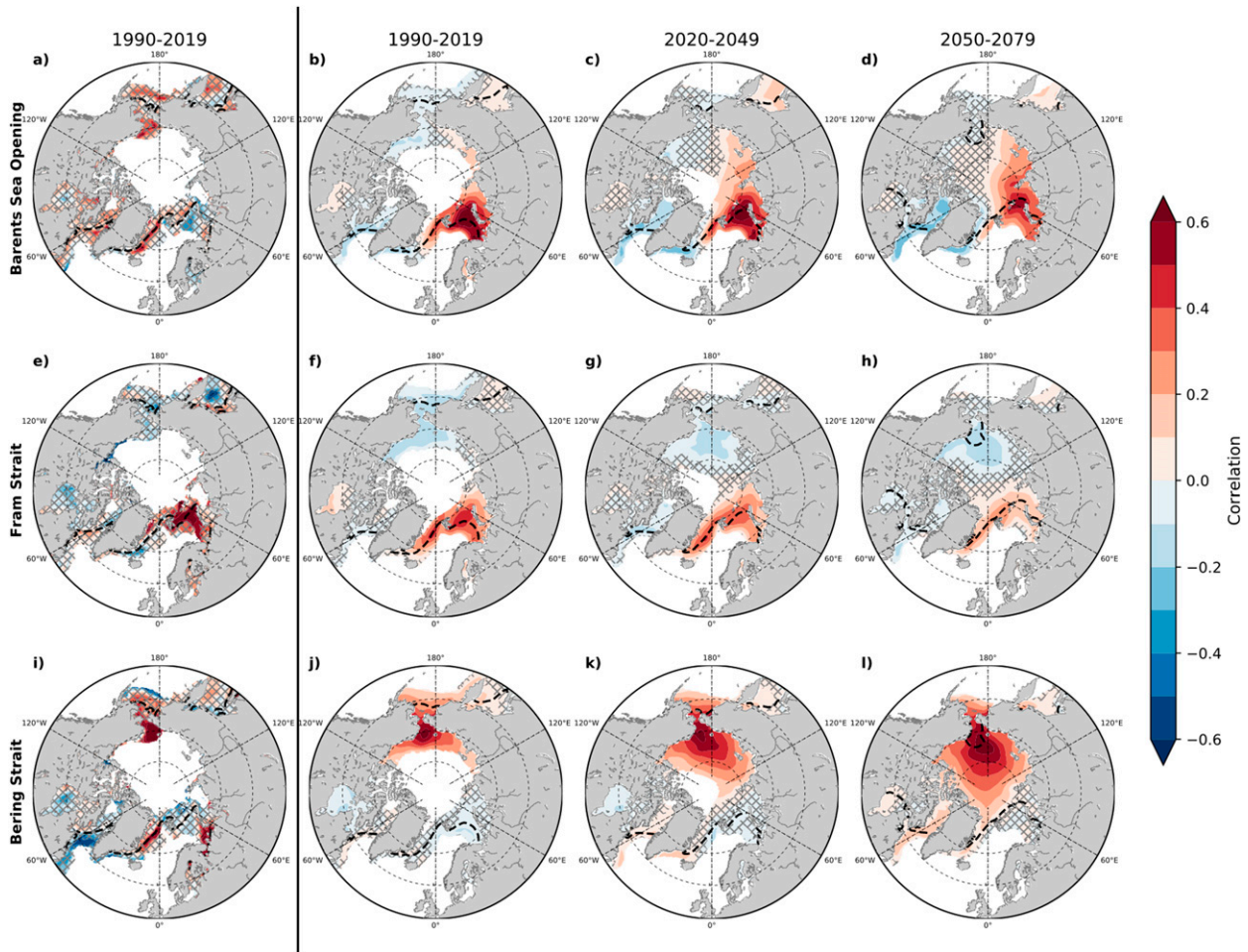


FIG. 5. Maps showing correlation between the annual mean ocean heat transport and following winter sea ice concentration in observations (left of black line) and three periods in CESM-LE (right of black line) for the (a)–(d) Barents Sea Opening, (e)–(h) Fram Strait, and (i)–(l) Bering Strait. Values are multiplied by -1 to reflect sea ice loss. Hatching indicates nonsignificant values at the 95% confidence interval. Points that are mostly ice-covered for each period (median more than 95%) are also removed. Black dashed contour indicates the mean sea ice edge based on a threshold of 50%. Correlations correspond to a lag of about 6 months between winter sea ice and heat transport.

waters below the mixed layer, except for the westernmost part of the section, around the ice edge northwest of Svalbard. The strongest correlations are found at depths of 200–300 m northwest of Svalbard, sinking toward 500 m at 100°E , before the influence weakens in the Eurasian Basin. The correlations generally increase from 1990–2019 to 2020–49, although remaining weak in the surface mixed layer. This weak surface influence is consistent with the weak influence of variable Fram Strait heat transport on the sea ice in the northern Barents Sea and southern Eurasian Basin (Figs. 5f–h). The limited influence on the surface layers north of Svalbard can be explained by a continuous presence of sea ice and a cold, well-mixed low-salinity surface layer overlying the Atlantic water.

Despite the weak influence of Fram Strait heat transport on surface layer temperatures, its impact on the sea ice in the first period is similar to the influence of the BSO heat transport, especially in the Barents Sea. This can be explained by a fairly

strong correlation ($R \sim 0.5$) between the two heat transports until around 2010 (Fig. 8). From the early 2000s, the correlation drops significantly, which coincides with a weakening influence of the Fram Strait heat transport on the sea ice in the two future periods. This suggests that the apparent influence of the Fram Strait heat transport on the sea ice in Figs. 5 and 6 is mainly an indirect influence via the BSO heat transport. The loss of covariability between the Barents and Fram Strait branch is further discussed in section 5c.

c. Bering Strait

On the other side of the Arctic Ocean, observations show that enhanced heat transport through the Bering Strait is associated with reduced sea ice concentration in the southern Chukchi Sea the following winter (Fig. 5i). The sea ice response to OHT appears most prominent in November–December (not shown) and is consistent with Serreze et al. (2016), who found a

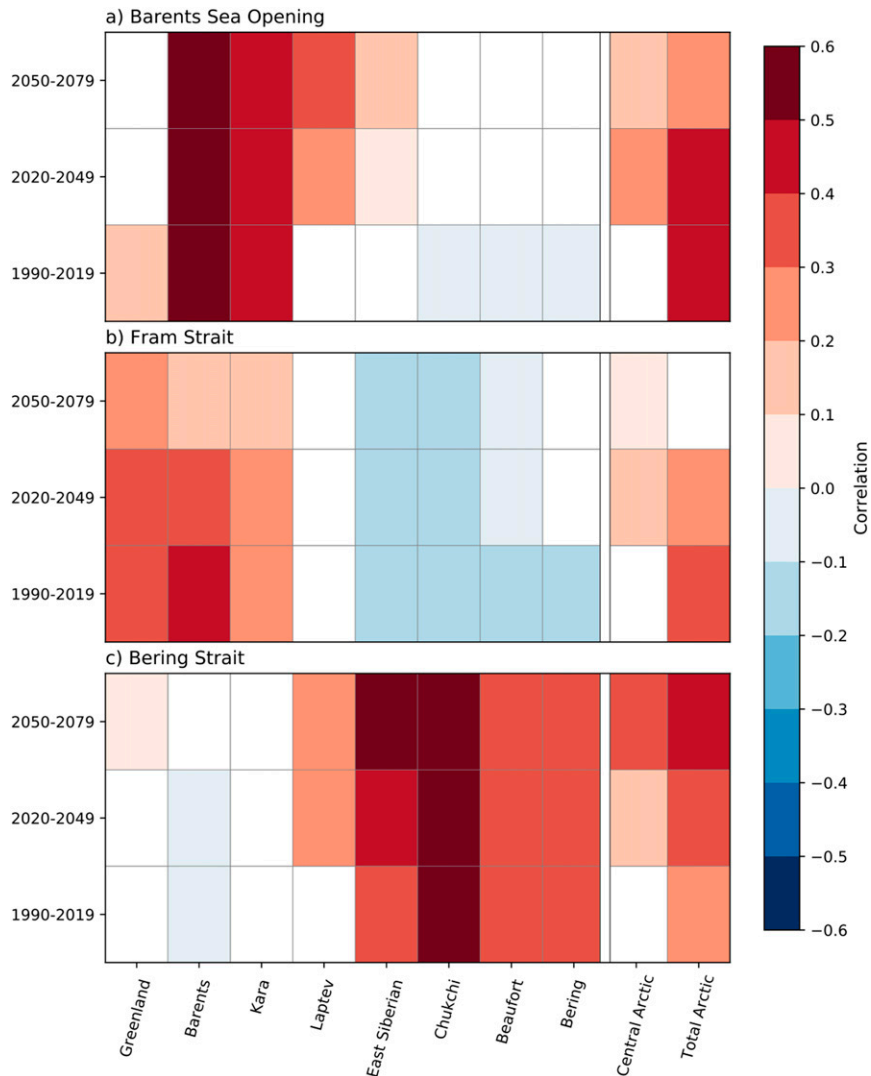


FIG. 6. Ocean heat transport driving winter sea ice variability. Correlation between regional winter (November–March) sea ice area in the Arctic Ocean and annual mean ocean heat transport through (a) Barents Sea Opening, (b) Fram Strait, and (c) Bering Strait in CESM-LE. Values are multiplied by -1 to reflect sea ice loss. Nonsignificant values at the 95% confidence interval are removed (white). Correlations correspond to a lag of about 6 months between winter sea ice and heat transport.

connection between the Chukchi freeze-up date and summer Bering Strait heat transport. We find a similar pattern in CESM-LE (Fig. 5j), with the biggest influence in the southern Chukchi Sea. For the future, the CESM-LE projects a large expansion of the region of Bering Strait influence into the central Arctic Ocean, with the highest correlations in the northern Chukchi Sea, the East Siberian Sea, the western Beaufort Sea, and the Pacific side of the Central Arctic Basin (Figs. 5k,l and 6c). For the last time period (2050–79), the influence of the Bering Strait heat transport on the total Arctic sea ice area surpasses that of the BSO heat transport.

Larger Bering Strait heat transport is associated with higher water temperatures above the Chukchi shelf as well as

in the surface mixed layer above the Canadian Basin, and with lower temperatures below the mixed layer and down to approximately 300 m in the Canadian Basin (Figs. 7g–i). This pattern of influence is consistent with the notion that the relatively warm Pacific waters enter the shallow Chukchi Shelf in summer (Woodgate et al. 2010, 2012; Serreze et al. 2016). When they meet the ice edge, they sink below the mixed layer, where they are colder, but less saline and therefore lighter, than the Atlantic-origin waters below. As the winter ice edge retreats toward the interior Arctic Ocean, more Pacific water can enter the Arctic Ocean in the surface mixed layer, which is reflected in the expanding future influence of the Bering Strait heat transport on mixed-layer temperatures and sea ice cover (Figs. 5k,l). This strong

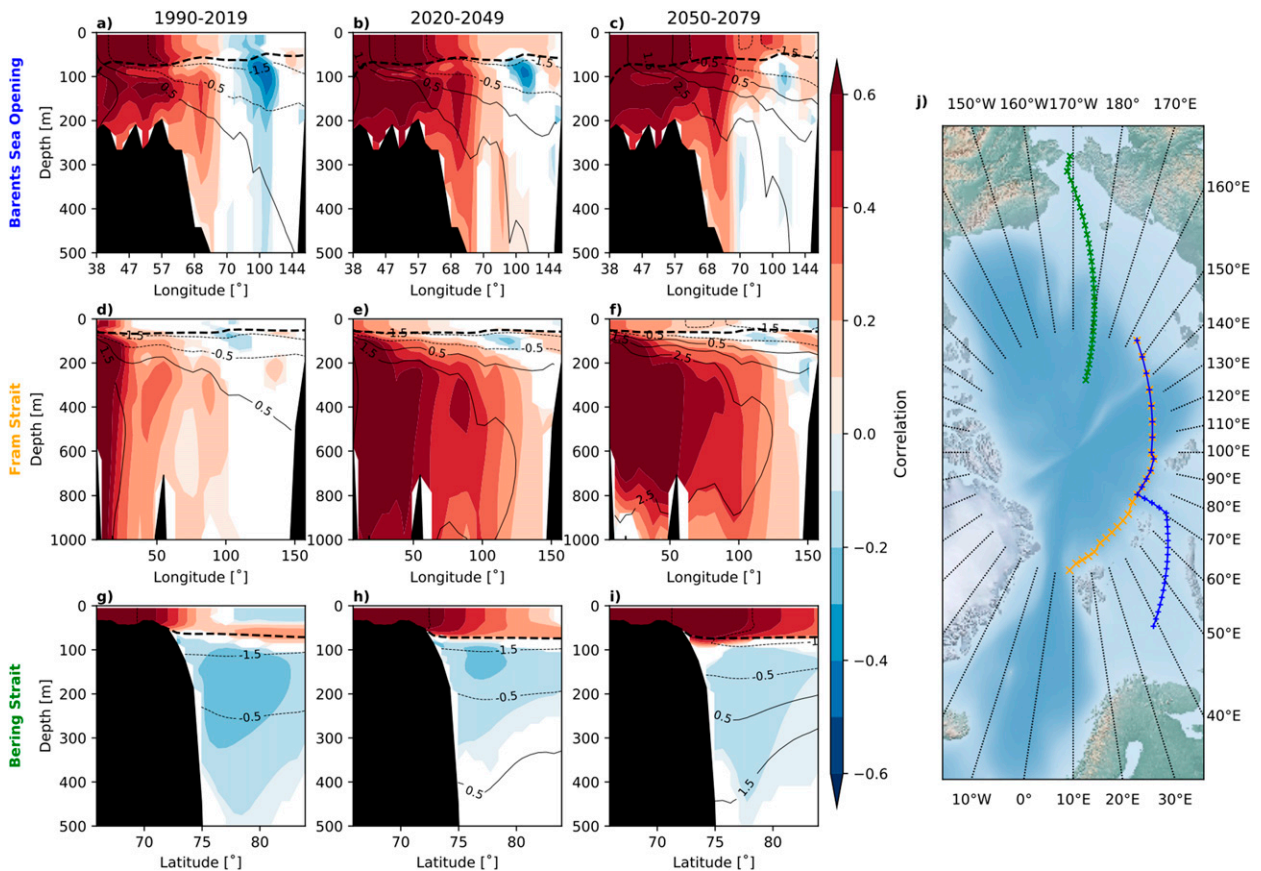


FIG. 7. (a)–(i) Correlation between annual mean ocean heat transport and winter (November–March) temperature along vertical sections (depicted in the map) for three different periods in CESM-LE. Nonsignificant values at the 95% confidence interval are removed. Black dashed contour indicates the ensemble mean winter surface mixed layer and thin dashed lines with label indicate the ensemble mean temperature. Correlations correspond to a lag of about 6 months between winter temperature and heat transport.

surface influence compared to the BSO and Fram Strait heat transports can explain the stronger influence on the total sea ice area in the future (Fig. 6).

5. The role of the atmosphere in winter sea ice variability

a. Hemispheric modes of variability

We begin the analysis by correlating the principal components of the two leading modes of hemispheric atmospheric variability, the AO and PNA* (Figs. 4c–f), and the time series of regional sea ice areas. The relationship between the two modes and the regional sea ice area variability is weak both for the recent past and in future periods in CESM-LE (Fig. 9) and in observations (not shown). A limited connection between the AO and winter sea ice area over the recent past is consistent with the findings of Wang and Ikeda (2000) and Wang et al. (2019b). Future interannual variability in regional sea ice areas on the Pacific side is weakly negatively correlated with the AO and weakly positively correlated with the PNA*, which means that lower sea ice areas are connected to lower pressure over the North Pacific, and easterly wind anomalies over the Pacific side (Figs. 4e,f).

b. Regional patterns of atmospheric influence

Because regional sea ice variability is found to be more connected to regional atmospheric circulation modes, we next compare and contrast those regional modes for the different regions, as well as for the recent past and future periods. To detect atmospheric circulation patterns connected to the regional sea ice variability we regress the time series of winter sea ice area onto winter sea level pressure and low-level winds. Because of similar sea ice variability and response to atmospheric forcing, we group the regions into the Atlantic side (Barents and Kara Seas), Pacific side (Bering, Chukchi, Beaufort, East Siberian Seas), and central Arctic (Central Basin, Laptev Sea). Regression patterns performed separately for all regions can be found in Fig. S2 in the online supplemental material.

During 1990–2019, in both ERA5 and CESM-LE, lower sea ice areas on the Atlantic side are associated with lower pressure over the northern Nordic seas and southerly winds in the Barents Sea (Figs. 10a,b). The center of the low pressure is weaker and centered farther southwest in CESM-LE. CESM-LE also shows a prominent high pressure over western Siberia, which is weaker in ERA5. For the Pacific side, both observations and CESM-LE feature high pressure over Alaska and low

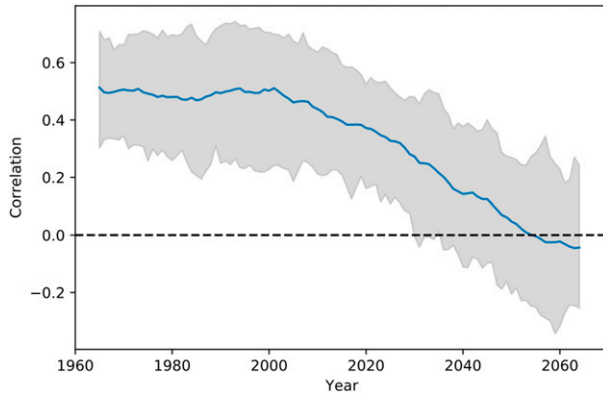


FIG. 8. Relationship between ocean heat transport through the Barents Sea and Fram Strait. Running 30-yr anomaly correlation between the annual mean Fram Strait heat transport and the annual mean Barents Sea heat transport in CESM-LE. Solid line represents ensemble mean and shading represents the interdecile member spread.

pressure over the southern Bering Sea associated with a lower sea ice area. The atmospheric circulation patterns driving Pacific and Atlantic sea ice variability are similar to those identified by Blackport et al. (2019) for the Barents–Kara and Bering–Chukchi Seas, respectively, using the CMIP5 version of the HadGEM2-ES model. For the Barents–Kara Seas, the results are also consistent with recent studies pointing at a connection between sea ice loss and a blocking high over the Ural region in combination with a positive phase of the North Atlantic Oscillation (Luo et al. 2017, 2016; Gong and Luo 2017), resulting

in a dipole pattern with low pressure over the Nordic seas and high pressure over the Ural region. We note that we find the low pressure more centered over the northern Nordic seas. Results from CESM-LE are thus in broad agreement with both ERA5 and other climate models. For the central Arctic, the anomalous atmospheric circulation in CESM-LE consists of high pressure over Eurasia and a broad low pressure pattern over America, while ERA5 shows low pressure south of Greenland and over eastern Europe. Southerly winds in the Atlantic sector associated with lower central Arctic sea ice area in CESM-LE (and to a lesser extent also in ERA5) are consistent with sea ice variability over this period mostly taking place northeast of Svalbard (Figs. 2a,b).

A key influence of the atmosphere on sea ice is through the advection of heat and moisture from midlatitudes, which impacts the air temperature, cloud cover, and downwelling radiation (e.g., Vihma et al. 2016; Woods and Caballero 2016; Hegyi and Taylor 2017). The cyclonic circulation associated with the low pressure system in the Atlantic sector (Figs. 10a–d) brings warm and humid air from midlatitudes into the Barents and Kara Seas, and the corresponding variability in surface air temperature and moisture is significantly connected to sea ice area changes over the Atlantic sector (Figs. S3a,b). Similarly, sea ice area changes over the Pacific sector are connected to variability in temperature and moisture over the North Pacific, where the Aleutian low conveys moisture into the Arctic (Figs. S3c,d). In both sectors the positive correlations of moisture and temperature with sea ice are locally constrained. Another influence is the direct wind forcing of sea ice drift and the surface ocean currents (e.g., Rigor et al. 2002), which we assess using the surface winds regressed onto the regional sea ice area (Fig. 10). In most cases, the winds match

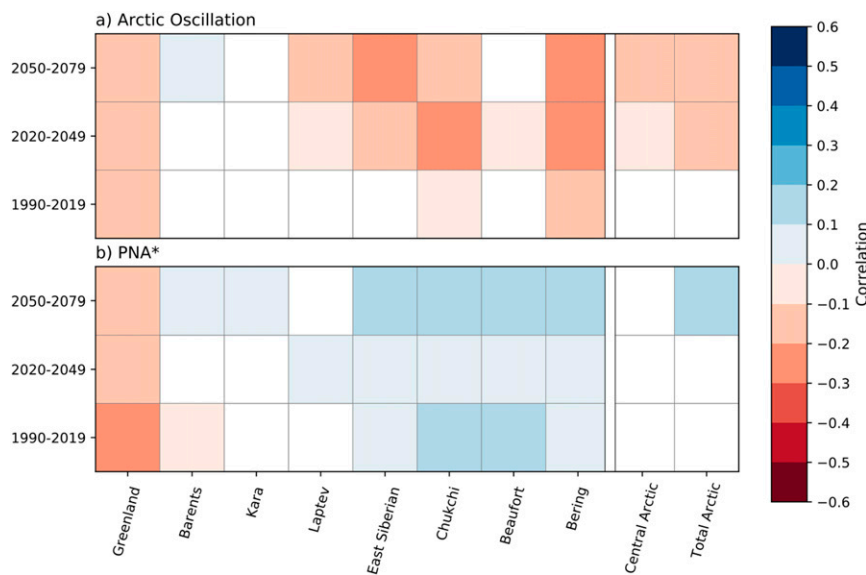


FIG. 9. Large-scale atmospheric forcing of sea ice variability. Correlation between the two dominant modes of winter (November–March) atmospheric circulation in the Arctic—(a) the Arctic Oscillation (AO) and (b) the Pacific North American pattern (PNA*)—with regional winter mean sea ice areas for three different periods in CESM-LE. Values are multiplied by -1 to reflect sea ice loss. Nonsignificant values at the 95% confidence interval are removed (white).

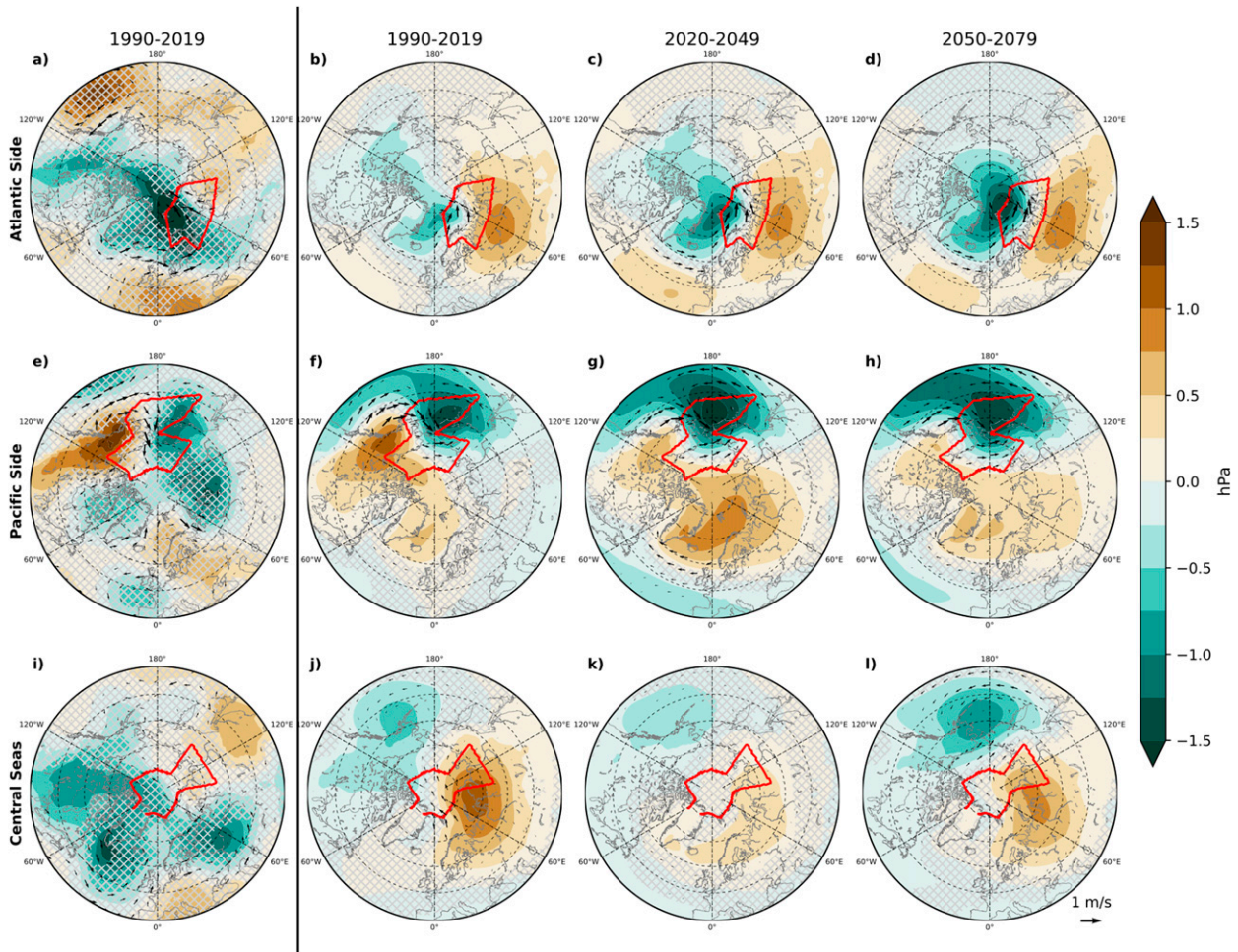


FIG. 10. Atmospheric circulation associated with regional winter sea ice variability. Regression coefficients between winter regional sea ice area and the winter mean sea level pressure (color shading) and surface winds (vectors) for (a)–(d) the Atlantic side, (e)–(h) the Pacific side, and (i)–(l) the central Arctic for ERA5 over the period 1990–2019 (left of black line) and CESM-LE over the periods 1990–2019, 2020–49, and 2050–79 (right of black line). Regression coefficients have units of $\text{hPa} (\text{m s}^{-1})$ per standard deviation of sea ice area anomalies and are multiplied by -1 to reflect sea ice loss. Hatching indicates nonsignificant values at the 95% confidence interval. Regions are indicated by the red contour.

the moisture and heat advection pathways. However, we also find easterly winds over the northern Chukchi Sea and the East Siberian Sea associated with sea ice variability on the Pacific side in CESM-LE (Figs. 10f–h). These winds are unlikely to be connected to heat and moisture advection, but rather to wind-forced movement of sea ice into the western Chukchi and East Siberian Seas.

In future periods, the sea level pressure pattern for the Atlantic side slightly changes toward lower pressure over the northern Barents Sea (Figs. 10c,d). For the Pacific side (Figs. 10g,h), the low pressure over the Aleutian Islands becomes deeper, indicating the importance of variability in the Aleutian low. The pattern for the central Arctic (Figs. 10k,l) remains similar and appears as a mix between the patterns for the Atlantic side (Siberian high) and Pacific side (Aleutian low).

To further assess the regional impact of wind-driven sea ice motion, we calculate the sea ice area export through Fram

Strait. A major feature of Arctic sea ice motion is the transpolar drift (Rudels 2015), and the associated sea ice area export through Fram Strait has been found to influence Arctic summer sea ice (Smedsrud et al. 2011). There is negligible correlation of regional sea ice area with winter Fram Strait sea ice export for the recent past in CESM-LE, except for the Greenland Sea (Fig. S4). However, there is a moderate negative relationship between the annual mean sea ice export and the Siberian shelf seas for future periods. This implies an influence of wind-driven sea ice motion in spring on sea ice conditions in the following winter.

c. Atmospheric influence on ocean heat transport

Atmospheric circulation variability can influence the Arctic sea ice cover; it can also impact ocean circulation, and hence ocean heat transport. We therefore investigate the relationship between anomalous atmospheric circulation and ocean heat

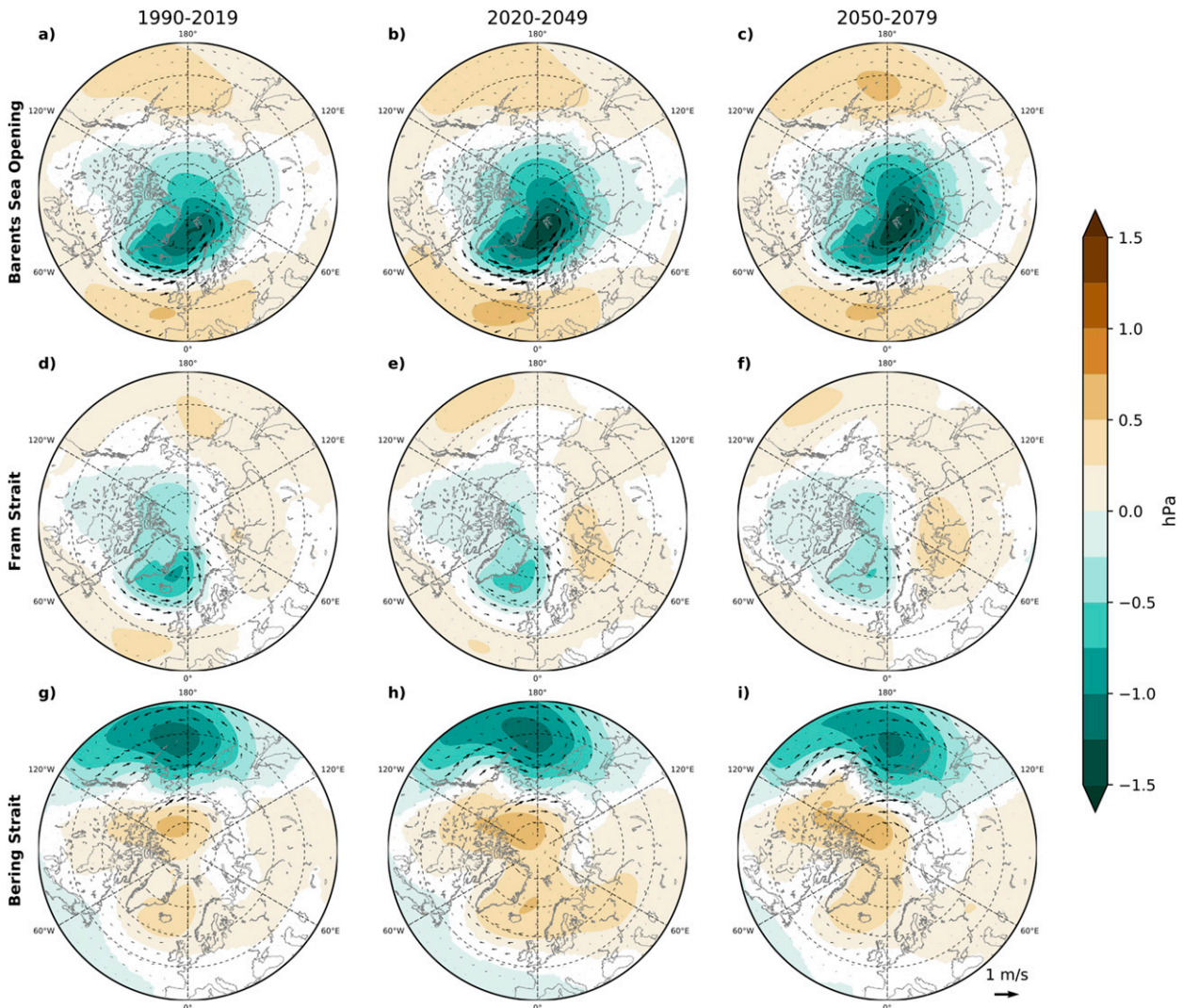


FIG. 11. Atmospheric circulation associated with variable ocean heat transport. Regression coefficients of annual mean ocean heat transport and with annual mean sea level pressure (color shading) and surface winds (vectors) for the (a)–(c) Barents Sea Opening, (d)–(f) Fram Strait, and (g)–(i) Bering Strait for three different periods in CESM-LE. Regression coefficients have units of hPa (m s^{-1}) per standard deviation of heat transport anomalies. Nonsignificant values at the 95% confidence interval are removed (white).

transport variability in CESM-LE by regressing the annual mean sea level pressure and surface winds onto the annual mean ocean heat transport through the BSO, Fram Strait, and Bering Strait.

The BSO heat transport is associated with low pressure over the Nordic seas and southwesterly winds along the Norwegian coast and into the Barents Sea (Figs. 11a–c). This is consistent with previous studies assessing the atmospheric influence on BSO heat transport and temperature (Skagseth et al. 2008; Muilwijk et al. 2019). Additionally, northerly winds in the Labrador Sea are likely the cause of the small positive correlations of sea ice concentration and BSO heat transport in this region (Figs. 5b–d). The regression pattern show a deepening and northeastwards extension of the low pressure system toward the northern Barents Sea in future periods.

The Fram Strait heat transport is associated with a similar pattern as the BSO heat transport (Fig. 11d), but with the low pressure centered more southward in the Iceland Sea causing the surface winds to blow northward through the eastern Fram Strait. Additionally, there is a region of high pressure over the Kara Seas, which hints at blocking over the eastern Barents Sea and Kara Sea that acts to divert cyclones into the Fram Strait (Madonna et al. 2020). Low pressure over the Greenland Sea and the associated positive wind stress curl is also a driver of a stronger Greenland Sea Gyre, which influences the strength and temperature of the northward flow of Atlantic Water in the Fram Strait (Chatterjee et al. 2018). In the future periods (Figs. 11e,f), the regression shows a strengthening of the high pressure and a weakening of the low pressure.

The similar atmospheric patterns of the Fram Strait and BSO heat transports provides a likely explanation of the correlation

between the two (Fig. 8). In future periods, however, the center of the atmospheric pattern associated with BSO heat transport shifts toward the Barents Sea (Figs. 11b,c), and the associated northerly winds west of Svalbard increase. This change can explain the decrease in correlation between the two heat transports projected by the CESM-LE.

The Bering Strait heat transport (Figs. 11g–i) is associated with high pressure over the central Arctic Ocean, and low pressure over the North Pacific, with a meridional pressure gradient along Bering Strait. This leads to easterly winds south of Alaska and in the Bering Sea, as well as in the Chukchi and East Siberian Seas. Through Ekman transport, such a wind pattern creates a sea surface height gradient from the Bering Sea toward the Chukchi Sea, which enhances the transport through the Bering Strait. This is consistent with previous work that suggests that the Bering Strait volume and heat transport are largely driven by variations in the large-scale wind patterns (Woodgate et al. 2012; Serreze et al. 2019). The regression pattern does not change substantially in future periods.

6. Influence of river runoff

Increased river runoff into the Arctic Ocean in summer can impact winter sea ice either through heat import (Park et al. 2020), or by adding surface freshwater, altering the stratification (Nummelin et al. 2016; Lambert et al. 2019). The correlation between the salinity at 5-m depth and single rivers reveals some local influence (more runoff → lower salinity; not shown). However, the correlation of the annual mean river runoff with the mean winter sea ice concentration reveals only a weak connection between the two, with maximum correlations of less than 0.15 across the Arctic (not shown). Although there are significant correlations in some areas, those areas are too far away from the source rivers to be directly impacted by the rivers, and the correlation is likely connected to atmospheric patterns that influence both the river runoff and the winter sea ice (e.g., the AO; Nummelin et al. 2016).

Although modeling experiments suggest a possible influence of river runoff variability on sea ice variability (Nummelin et al. 2016; Park et al. 2020), our results show that this influence is small compared with other sources of internal variability in the model. We note, however, that CESM-LE most likely underestimates the influence of river runoff on sea ice variability, as the river runoff is assumed to enter with the local ocean temperature. The impact of river heat input is thus not captured.

7. Interannual variability versus trends

In this work, we have focused on internal variability on interannual time scales, but Arctic sea ice also displays internal variability on longer time scales (Day et al. 2012; Zhang 2015; Årthun et al. 2019). To compare the atmospheric and oceanic influence on short and long time scales, we show in Fig. 12 the ensemble trend regressions of the main atmospheric and oceanic drivers of sea ice variability onto the sea ice area in the Chukchi–East Siberian Seas (Pacific) and Barents–Kara Seas (Atlantic) for the period 2045–80, considering trend lengths

between 5 and 30 years. We choose the ocean heat transport through the BSO and the Bering Strait to represent the oceanic drivers, and sea level pressure north of Svalbard and in the Bering Sea to represent the Nordic seas and Aleutian lows, respectively, following the regression patterns in Figs. 10a–f. Please recall that trends analyzed here result only from internal variability, as the ensemble mean (the forced trend) has been removed from each member.

For the annual mean ocean heat transports, we obtain similar negative correlation values for all the analyzed time scales. The ensemble trend correlations are higher than that found for interannual variability, and thus indicates a similar but stronger influence of ocean heat transport on longer time scales. For the atmospheric influence, the correlations are lower than for the ocean heat transports. The correlation is roughly constant for all time scales for the Nordic seas low, whereas the correlation for the Aleutian low decreases and reverses sign for trends longer than 20 years. Thus, the atmospheric influence on the Atlantic side is consistent for short and long time scales, while different mechanisms are at play on the Pacific side for long time scales. A detailed analysis of possible mechanisms of low-frequency atmospheric variability is beyond the scope of this study. We note, however, that the sea level pressure pattern associated with 30-yr trends resembles that associated with the Pacific decadal oscillation (not shown), which captures low-frequency variability in the Aleutian low (Di Lorenzo et al. 2010) and which in turn is known to influence Arctic climate (Svendsen et al. 2018).

8. Discussion and conclusions

In this study, we have assessed the connection of the regional winter sea ice variability in the Arctic to the oceanic and atmospheric circulation variability in the present and the future, using a combination of available observations and CESM-LE. CESM-LE largely agrees with observations on the spatial and temporal distribution of sea ice variability, as well as the mean state and recent trends. Both observations and CESM-LE show similar patterns of oceanic and atmospheric connections to winter sea ice for the Bering Sea and Barents Sea, the main regions of variability over the recent past, indicating that CESM-LE is able to capture these connections, providing confidence in the model's ability to assess future changes.

In agreement with previous studies, we find that ocean heat transport has been a major driver of recent sea ice variability in the Atlantic (Årthun et al. 2012; Lien et al. 2017) and Pacific sector (Woodgate et al. 2012; Serreze et al. 2016). The footprints of the Atlantic and Pacific inflows expand in the future, their combined influence covering a large part of the Arctic Ocean in 2050–79.

We find that present winter sea ice only weakly covaries with hemispheric large-scale atmospheric circulation modes (AO, PNA*), but it covaries with distinct localized atmospheric circulation patterns connected to regional sea ice variability (Fig. 10), similar to the findings of Luo et al. (2017), Gong and Luo (2017), and Blackport et al. (2019). Moreover, we show that such relationships hold also in the future. Furthermore, we find little influence of river runoff variability on winter sea ice

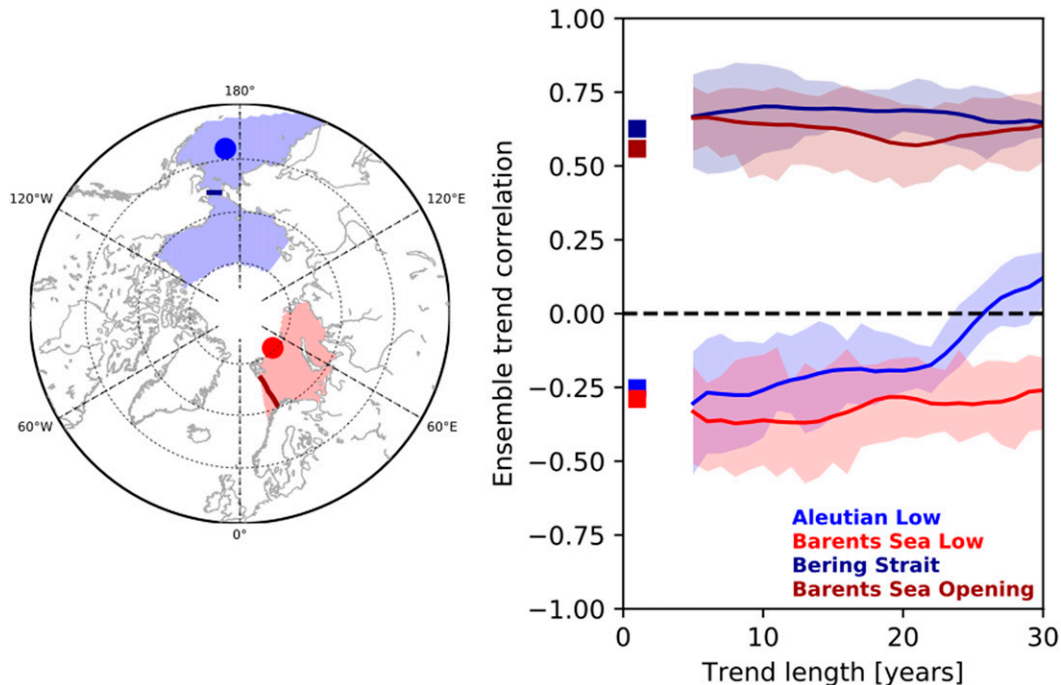


FIG. 12. (right) Ensemble trend regression between regional sea ice area in the Atlantic (Pacific) side and ocean heat transport through the Barents Sea Opening (Bering Strait) in CESM-LE, and between sea ice area and regional sea level pressure variability represented by the Barents Sea low (Aleutian low; see Fig. 10). The sea ice regions (shading), heat transport sections (lines), and sea level pressure points (filled circles) are shown on the map. Correlations are calculated for different trend lengths for the period 2045–79. Shading on the graph represents interdecile range over all possible periods during 2045–79. Squares indicate the anomaly correlation for interannual time scales over the same period. Values are multiplied by -1 to reflect sea ice loss.

in the context of internal variability in the fully coupled CESM-LE.

A schematic illustrating the different regional footprints of oceanic and atmospheric forcing on winter Arctic sea ice and their projected future changes is presented in Fig. 13. For both the oceanic and atmospheric drivers, we find distinct similarities in their regional influence on sea ice in the Atlantic and Pacific sectors of the Arctic, with the border between the two sectors roughly in the Laptev Sea. This border represents the topographically constrained location of the front between the Atlantic and Pacific haloclines (Rudels et al. 1994). The Atlantic side is influenced by oceanic and atmospheric advection of heat and moisture via the Barents Sea, while the Pacific side is influenced by advection from the northern Pacific and through the Bering Strait (Figs. 5 and 10; see also Fig. S3). These pathways are largely consistent with the flow of Atlantic Water (Rudels et al. 2015) and Pacific Water (Aksenov et al. 2016). For the Atlantic side, the atmospheric mode and advection pathways in the left panel of Fig. 13 is furthermore consistent with those found by Luo et al. (2017) (their Fig. 8) and Gimeno et al. (2019) (their Fig. 3). The future increase in footprint is especially large for the Bering Strait ocean heat transport, which can be explained by warm Pacific Water entering in the surface layers (Fig. 7) thus impacting the sea ice more efficiently than the Atlantic inflow (Docquier et al. 2021). The future relationships between winter sea ice and the oceanic and atmospheric forcing

assessed here are similar on interannual and decadal time scales, except for the atmospheric influence in the North Pacific.

We have also shown that the surface wind patterns associated with oceanic heat transport through the different gateways are similar to the patterns directly connected to sea ice area variability in the regions influenced by the heat transports, indicating a connection between atmospheric and oceanic influence on the sea ice. This is most visible for the BSO heat transport, as seen by the similarity of Figs. 10a–d and 11a–c. Atmospheric variability on the Atlantic side is thus influencing sea ice not only directly through heat and moisture transport, but also indirectly by driving ocean heat transport through BSO and Fram Strait. This creates covariability between the BSO and Fram Strait heat transports, which is reduced in future periods as the atmospheric regression patterns change. Similarly, on the Pacific side, easterly winds in the northern Chukchi Sea and the East Siberian Sea are associated both with changes in the local sea ice area and the Bering Strait heat transport (Figs. 10f–h and 11g–i). The close connection between sea ice variability, atmospheric circulation, and ocean heat transport is also true for decadal time scales, both for the Barents Sea (Ikeda 1990) and Chukchi Sea (Shimada et al. 2006), and has been explained by the existence of positive feedback mechanisms. Such feedback mechanisms have nevertheless been hard to demonstrate in fully coupled climate models (Smedsrud et al. 2013) and are not assessed here.

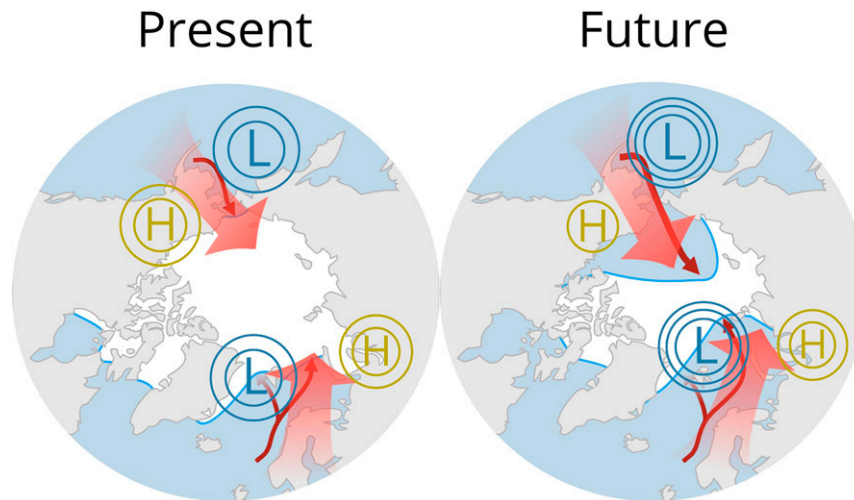


FIG. 13. Illustration of the major drivers of winter sea ice reduction in CESM-LE for the (left) present and (right) future, including oceanic (dark red arrows) and atmospheric (light red arrows) pathways of heat and moisture, and dominant large-scale sea level pressure patterns (H and L).

We have used annual averages for the oceanic heat transport to account for the integrated signal of oceanic influence on the winter sea ice. Repeating the analysis with seasonal averages (not shown) reveals that for the BSO, the future poleward expansion of influence mainly stems from heat transport anomalies in late winter and spring. This is consistent with strongest BSO heat transport in winter (Fig. S1; [Årthun et al. 2012](#)), which influences spring ice melt and summer temperatures in the Barents Sea, and which in turn influences the sea ice in the freezing season ([Ottersen et al. 2000](#); [Schlichtholz 2011](#)). In contrast, the influence of the Bering Strait heat transport mainly stems from summer when the passage is ice-free and heat transport is strongest (Fig. S1), influencing water temperatures and delaying freeze-up ([Serreze et al. 2016](#)). For the atmospheric circulation variability we focused on the direct influence in winter. However, the atmospheric impact on spring sea ice melt and summer sea surface temperatures is also important for sea ice freeze-up in autumn and winter ([Blanchard-Wrigglesworth et al. 2011](#); [Bushuk and Giannakis 2017](#)). As the freeze-up for the central Arctic Ocean moves into early winter (Figs. 2c,d), this influence is expected to become more important for the winter sea ice in these regions.

Our results rely on correlation and regression between the different oceanic and atmospheric variables and the winter sea ice. We recognize that such analysis cannot be used to unequivocally infer the causal influence of these variables on the sea ice. This applies especially for the atmospheric circulation in winter, as it is still debated how much the sea ice itself is influencing atmospheric circulation patterns ([Vihma 2014](#); [Zhong et al. 2018](#); [Blackport and Screen 2020](#); [Cohen et al. 2020](#)). However, recent studies suggest that on interannual time scales (the focus of this study) the influence of sea ice variability on atmospheric circulation variability has so far been limited ([Blackport et al. 2019](#); [Warner et al. 2020](#)). To assess whether this finding also holds for the future Arctic is beyond the scope of our study.

The agreement between observations and CESM-LE on the present atmospheric and oceanic mechanisms of winter sea ice variability (Figs. 4, 5, and 10) provides confidence in our results. It was also noted by [Årthun et al. \(2019\)](#) that the relationship between the ocean heat transport through the BSO and the sea ice in the Barents Sea is realistic. We nevertheless acknowledge the limitations of using simulations from a single climate model. The stratification and vertical mixing in the upper ocean, which influences the transfer of subsurface heat to the ice cover ([Carmack et al. 2015](#)), are difficult to capture with coarse-resolution models ([Lique et al. 2016](#)). This has consequences for the simulated influence of Atlantic and Pacific water on the sea ice, as well as the effect of river runoff on the water column ([Lambert et al. 2019](#)). Furthermore, biases in the winter atmospheric circulation could also affect our results on the importance of large-scale circulation patterns. We note, however, that the CESM-LE adequately captures winter atmospheric circulation variability ([Wang et al. 2019a](#)).

Our findings demonstrate the importance of atmospheric and oceanic drivers for present and future Arctic winter sea ice variability, and thus detail the future progression of the ongoing Atlantification of the eastern Arctic ([Årthun et al. 2012](#); [Polyakov et al. 2017](#)) and a pronounced future Pacification of the Pacific side of the Arctic Ocean. Our results also improve our understanding of internal climate variability, which is essential in order to predict future sea ice changes under anthropogenic warming.

Acknowledgments. This study was funded by the Research Council of Norway projects Nansen Legacy (Grant 276730), the Blue-Action project (European Union's Horizon 2020 research and innovation program; Grant 727852), and the Trond Mohn Foundation (Grant BFS2018TMT01). Furthermore, we thank the CESM Large Ensemble Community Project for making their data publicly accessible. We thank three anonymous reviewers for constructive suggestions that improved the manuscript.

Data availability statement. All data in this study are publicly available. OSI SAF gridded sea-ice concentration are available at <https://osi-saf.eumetsat.int/products/sea-ice-products>. Output from ERA5 is available through the Copernicus Climate Change Service: <https://cds.climate.copernicus.eu/cdsapp#!/dataset/10.24381/cds.f17050d7>. Output from CESM-LE is available via the Earth System Grid: <https://www.earthsystemgrid.org>. Observed Bering Strait ocean heat transport data are available at <http://psc.apl.washington.edu/HLD/Bstrait/bstrait.html>. Monthly Fram Strait (West Spitsbergen Current) volume transport data are available at <http://www.oceansites.org/tma/fram.html> and temperature data are available at <https://ocean.ices.dk/core/iroc>. The observed BSO heat transport data are available at ftp://ftp.nmdc.no/nmdc/IMR/fastesnitt/indexs/fluks_mnd_1997_2017.xls.

REFERENCES

- Aagaard, K., L. K. Coachman, and E. Carmack, 1981: On the halocline of the Arctic Ocean. *Deep-Sea Res.*, **28**, 529–545, [https://doi.org/10.1016/0198-0149\(81\)90115-1](https://doi.org/10.1016/0198-0149(81)90115-1).
- Aksenov, Y., and Coauthors, 2016: Arctic pathways of Pacific water: Arctic Ocean Model Intercomparison experiments. *J. Geophys. Res. Oceans*, **121**, 27–59, <https://doi.org/10.1002/2015JC011299>.
- Årthun, M., T. Eldevik, L. H. Smedsrud, Ø. Skagseth, and R. B. Ingvaldsen, 2012: Quantifying the influence of Atlantic heat on Barents Sea ice variability and retreat. *J. Climate*, **25**, 4736–4743, <https://doi.org/10.1175/JCLI-D-11-00466.1>.
- , —, and —, 2019: The role of Atlantic heat transport in future Arctic winter sea ice loss. *J. Climate*, **32**, 3327–3341, <https://doi.org/10.1175/JCLI-D-18-0750.1>.
- , I. H. Onarheim, J. Dörr, and T. Eldevik, 2021: The seasonal and regional transition to an ice-free Arctic. *Geophys. Res. Lett.*, **48**, e2020GL090825, <https://doi.org/10.1029/2020GL090825>.
- Auclair, G., and L. B. Tremblay, 2018: The role of ocean heat transport in rapid sea ice declines in the Community Earth System Model Large Ensemble. *J. Geophys. Res. Oceans*, **123**, 8941–8957, <https://doi.org/10.1029/2018JC014525>.
- Barnhart, K. R., C. R. Miller, I. Overeem, and J. E. Kay, 2016: Mapping the future expansion of Arctic open water. *Nat. Climate Change*, **6**, 280–285, <https://doi.org/10.1038/nclimate2848>.
- Beszczynska-Möller, A., E. Fahrbach, U. Schauer, and E. Hansen, 2012: Variability in Atlantic water temperature and transport at the entrance to the Arctic Ocean, 1997–2010. *ICES J. Mar. Sci.*, **69**, 852–863, <https://doi.org/10.1093/icesjms/fss056>.
- Blackport, R., and J. A. Screen, 2020: Weakened evidence for mid-latitude impacts of Arctic warming. *Nat. Climate Change*, **10**, 1065–1066, <https://doi.org/10.1038/s41558-020-00954-y>.
- , —, K. van der Wiel, and R. Bintanja, 2019: Minimal influence of reduced Arctic sea ice on coincident cold winters in mid-latitudes. *Nat. Climate Change*, **9**, 697–704, <https://doi.org/10.1038/s41558-019-0551-4>.
- Blanchard-Wrigglesworth, E., K. C. Armour, C. M. Bitz, and E. DeWeaver, 2011: Persistence and inherent predictability of Arctic sea ice in a GCM ensemble and observations. *J. Climate*, **24**, 231–250, <https://doi.org/10.1175/2010JCLI3775.1>.
- Bonan, D. B., F. Lehner, and M. M. Holland, 2021: Partitioning uncertainty in projections of Arctic sea ice. *Environ. Res. Lett.*, **16**, 044002, <https://doi.org/10.1088/1748-9326/abe0ec>.
- Bushuk, M., and D. Giannakis, 2017: The seasonality and inter-annual variability of Arctic sea ice reemergence. *J. Climate*, **30**, 4657–4676, <https://doi.org/10.1175/JCLI-D-16-0549.1>.
- Cai, L., V. A. Alexeev, and J. E. Walsh, 2020: Arctic sea ice growth in response to synoptic- and large-scale atmospheric forcing from CMIP5 models. *J. Climate*, **33**, 6083–6099, <https://doi.org/10.1175/JCLI-D-19-0326.1>.
- Carmack, E., and Coauthors, 2015: Toward quantifying the increasing role of oceanic heat in sea ice loss in the new Arctic. *Bull. Amer. Meteor. Soc.*, **96**, 2079–2105, <https://doi.org/10.1175/BAMS-D-13-00177.1>.
- , and Coauthors, 2016: Freshwater and its role in the Arctic marine system: Sources, disposition, storage, export, and physical and biogeochemical consequences in the Arctic and global oceans. *J. Geophys. Res. Biogeosci.*, **121**, 675–717, <https://doi.org/10.1002/2015JG003140>.
- Chatterjee, S., R. P. Raj, L. Bertino, Ø. Skagseth, M. Ravichandran, and O. M. Johannessen, 2018: Role of Greenland Sea gyre circulation on Atlantic water temperature variability in the Fram Strait. *Geophys. Res. Lett.*, **45**, 8399–8406, <https://doi.org/10.1029/2018GL079174>.
- Cohen, J., and Coauthors, 2020: Divergent consensus on Arctic amplification influence on midlatitude severe winter weather. *Nat. Climate Change*, **10**, 20–29, <https://doi.org/10.1038/s41558-019-0662-y>.
- Day, J. J., J. C. Hargreaves, J. D. Annan, and A. Abe-Ouchi, 2012: Sources of multi-decadal variability in Arctic sea ice extent. *Environ. Res. Lett.*, **7**, 034011, <https://doi.org/10.1088/1748-9326/7/3/034011>.
- Deser, C., J. E. Walsh, and M. S. Timlin, 2000: Arctic sea ice variability in the context of recent atmospheric circulation trends. *J. Climate*, **13**, 617–633, [https://doi.org/10.1175/1520-0442\(2000\)013<0617:ASIVIT>2.0.CO;2](https://doi.org/10.1175/1520-0442(2000)013<0617:ASIVIT>2.0.CO;2).
- Desmarais, A., and B. Tremblay, 2021: Assessment of decadal variability in sea ice in the Community Earth System Model against a long-term regional observational record: Implications for the predictability of an ice-free Arctic. *J. Climate*, **34**, 5367–5384, <https://doi.org/10.1175/JCLI-D-20-0561.1>.
- Di Lorenzo, E., K. M. Cobb, J. C. Furtado, N. Schneider, B. T. Anderson, A. Bracco, M. A. Alexander, and D. J. Vimont, 2010: Central Pacific El Niño and decadal climate change in the North Pacific Ocean. *Nat. Geosci.*, **3**, 762–765, <https://doi.org/10.1038/ngeo984>.
- Ding, Q., and Coauthors, 2017: Influence of high-latitude atmospheric circulation changes on summertime Arctic sea ice. *Nat. Climate Change*, **7**, 289–295, <https://doi.org/10.1038/nclimate3241>.
- , and Coauthors, 2019: Fingerprints of internal drivers of Arctic sea ice loss in observations and model simulations. *Nat. Geosci.*, **12**, 28–33, <https://doi.org/10.1038/s41561-018-0256-8>.
- Docquier, D., T. Koenigk, R. Fuentes-Franco, M. Pasha Karami, and Y. Ruprich-Robert, 2021: Impact of ocean heat transport on the Arctic sea-ice decline: A model study with EC-Earth3. *Climate Dyn.*, **56**, 1407–1432, <https://doi.org/10.1007/s00382-020-05540-8>.
- England, M., A. Jahn, and L. Polvani, 2019: Nonuniform contribution of internal variability to recent Arctic sea ice loss. *J. Climate*, **32**, 4039–4053, <https://doi.org/10.1175/JCLI-D-18-0864.1>.
- Francis, J. A., and E. Hunter, 2007: Drivers of declining sea ice in the Arctic winter: A tale of two seas. *Geophys. Res. Lett.*, **34**, L17503, <https://doi.org/10.1029/2007GL030995>.
- Gimeno, L., M. Vázquez, J. Eiras-Barca, R. Sorí, I. Algarra, and R. Nieto, 2019: Atmospheric moisture transport and the decline in Arctic sea ice. *Wiley Interdiscip. Rev.: Climate Change*, **10**, e588, <https://doi.org/10.1002/wcc.588>.
- Gong, H., L. Wang, W. Chen, X. Chen, and D. Nath, 2016: Biases of the wintertime Arctic Oscillation in CMIP5 models. *Environ.*

- Res. Lett.*, **12**, 014001, <https://doi.org/10.1088/1748-9326/12/1/014001>.
- Gong, T., and D. Luo, 2017: Ural blocking as an amplifier of the Arctic sea ice decline in winter. *J. Climate*, **30**, 2639–2654, <https://doi.org/10.1175/JCLI-D-16-0548.1>.
- Graham, R. M., and Coauthors, 2019: Evaluation of six atmospheric reanalyses over Arctic sea ice from winter to early summer. *J. Climate*, **32**, 4121–4143, <https://doi.org/10.1175/JCLI-D-18-0643.1>.
- Hausfather, Z., and G. P. Peters, 2020: Emissions—The ‘business as usual’ story is misleading. *Nature*, **577**, 618–620, <https://doi.org/10.1038/d41586-020-00177-3>.
- Hegyí, B. M., and P. C. Taylor, 2017: The regional influence of the Arctic Oscillation and Arctic dipole on the wintertime Arctic surface radiation budget and sea ice growth. *Geophys. Res. Lett.*, **44**, 4341–4350, <https://doi.org/10.1002/2017GL073281>.
- Hersbach, H., and Coauthors, 2020: The ERA5 global reanalysis. *Quart. J. Roy. Meteor. Soc.*, **146**, 1999–2049, <https://doi.org/10.1002/qj.3803>.
- Holland, M. M., and J. Stroeve, 2011: Changing seasonal sea ice predictor relationships in a changing Arctic climate. *Geophys. Res. Lett.*, **38**, L18501, <https://doi.org/10.1029/2011GL049303>.
- Ikeda, M., 1990: Decadal oscillations of the air–ice–ocean system in the Northern Hemisphere. *Atmos.–Ocean*, **28**, 106–139, <https://doi.org/10.1080/07055900.1990.9649369>.
- Ingvaldsen, R. B., L. Asplin, and H. Loeng, 2004: The seasonal cycle in the Atlantic transport to the Barents Sea during the years 1997–2001. *Cont. Shelf Res.*, **24**, 1015–1032, <https://doi.org/10.1016/j.csr.2004.02.011>.
- Jahn, A., and R. Laiho, 2020: Forced changes in the Arctic freshwater budget emerge in the early 21st century. *Geophys. Res. Lett.*, **47**, e2020GL088854, <https://doi.org/10.1029/2020GL088854>.
- , J. E. Kay, M. M. Holland, and D. M. Hall, 2016: How predictable is the timing of a summer ice-free Arctic? *Geophys. Res. Lett.*, **43**, 9113–9120, <https://doi.org/10.1002/2016GL070067>.
- Kay, J. E., and Coauthors, 2015: The Community Earth System Model (CESM) large ensemble project: A community resource for studying climate change in the presence of internal climate variability. *Bull. Amer. Meteor. Soc.*, **96**, 1333–1349, <https://doi.org/10.1175/BAMS-D-13-00255.1>.
- Kim, K.-Y., J.-Y. Kim, J. Kim, S. Yeo, H. Na, B. D. Hamlington, and R. R. Leben, 2019: Vertical feedback mechanism of winter Arctic amplification and sea ice loss. *Sci. Rep.*, **9**, 1184, <https://doi.org/10.1038/s41598-018-38109-x>.
- Lambert, E., A. Nummelin, P. Pemberton, and M. Ilıcak, 2019: Tracing the imprint of river runoff variability on Arctic water mass transformation. *J. Geophys. Res. Oceans*, **124**, 302–319, <https://doi.org/10.1029/2017JC013704>.
- Lavergne, T., and Coauthors, 2019: Version 2 of the EUMETSAT OSI SAF and ESA CCI sea-ice concentration climate data records. *Cryosphere*, **13**, 49–78, <https://doi.org/10.5194/tc-13-49-2019>.
- Lien, V. S., P. Schlichtholz, Ø. Skagseth, and F. B. Vikebø, 2017: Wind-driven Atlantic water flow as a direct mode for reduced Barents Sea ice cover. *J. Climate*, **30**, 803–812, <https://doi.org/10.1175/JCLI-D-16-0025.1>.
- Lind, S., and R. B. Ingvaldsen, 2012: Variability and impacts of Atlantic water entering the Barents Sea from the north. *Deep-Sea Res. I*, **62**, 70–88, <https://doi.org/10.1016/j.dsr.2011.12.007>.
- Lique, C., M. M. Holland, Y. B. Dibikey, D. M. Lawrence, and J. A. Screen, 2016: Modeling the Arctic freshwater system and its integration in the global system: Lessons learned and future challenges. *J. Geophys. Res. Biogeosci.*, **121**, 540–566, <https://doi.org/10.1002/2015JG003120>.
- Luo, B., D. Luo, L. Wu, L. Zhong, and I. Simmonds, 2017: Atmospheric circulation patterns which promote winter Arctic Sea ice decline. *Environ. Res. Lett.*, **12**, 054017, <https://doi.org/10.1088/1748-9326/aa69d0>.
- Luo, D., Y. Xiao, Y. Yao, A. Dai, I. Simmonds, and C. L. E. Franzke, 2016: Impact of Ural blocking on winter warm Arctic–cold Eurasian anomalies. Part I: Blocking-induced amplification. *J. Climate*, **29**, 3925–3947, <https://doi.org/10.1175/JCLI-D-15-0611.1>.
- Madonna, E., G. Hes, C. Li, C. Michel, and P. Y. F. Siew, 2020: Control of Barents Sea wintertime cyclone variability by large-scale atmospheric flow. *Geophys. Res. Lett.*, **47**, e2020GL090322, <https://doi.org/10.1029/2020GL090322>.
- Muilwijk, M., and Coauthors, 2019: Arctic Ocean response to Greenland Sea wind anomalies in a suite of model simulations. *J. Geophys. Res. Oceans*, **124**, 6286–6322, <https://doi.org/10.1029/2019JC015101>.
- Notz, D., and J. Stroeve, 2016: Observed Arctic Sea-ice loss directly follows anthropogenic CO₂ emission. *Science*, **354**, 747–750, <https://doi.org/10.1126/science.aag2345>.
- , and SIMIP Community, 2020: Arctic sea ice in CMIP6. *Geophys. Res. Lett.*, **47**, e2019GL086749, <https://doi.org/10.1029/2019GL086749>.
- Nummelin, A., M. Ilıcak, C. Li, and L. H. Smedsrud, 2016: Consequences of future increased Arctic runoff on Arctic Ocean stratification, circulation, and sea ice cover. *J. Geophys. Res. Oceans*, **121**, 617–637, <https://doi.org/10.1002/2015JC011156>.
- Nygård, T., T. Naakka, and T. Vihma, 2020: Horizontal moisture transport dominates the regional moistening patterns in the Arctic. *J. Climate*, **33**, 6793–6807, <https://doi.org/10.1175/JCLI-D-19-0891.1>.
- Olonscheck, D., T. Mauritsen, and D. Notz, 2019: Arctic sea-ice variability is primarily driven by atmospheric temperature fluctuations. *Nat. Geosci.*, **12**, 430–434, <https://doi.org/10.1038/s41561-019-0363-1>.
- Onarheim, I. H., L. H. Smedsrud, R. B. Ingvaldsen, and F. Nilsen, 2014: Loss of sea ice during winter north of Svalbard. *Tellus*, **66A**, 23933, <https://doi.org/10.3402/tellusa.v66.23933>.
- , T. Eldevik, M. Årthun, R. B. Ingvaldsen, and L. H. Smedsrud, 2015: Skillful prediction of Barents Sea ice cover. *Geophys. Res. Lett.*, **42**, 5364–5371, <https://doi.org/10.1002/2015GL064359>.
- , —, L. H. Smedsrud, and J. C. Stroeve, 2018: Seasonal and regional manifestation of Arctic sea ice loss. *J. Climate*, **31**, 4917–4932, <https://doi.org/10.1175/JCLI-D-17-0427.1>.
- Ottersen, G., B. Ådlandsvik, and H. Loeng, 2000: Predicting the temperature of the Barents Sea. *Fish. Oceanogr.*, **9**, 121–135, <https://doi.org/10.1046/j.1365-2419.2000.00127.x>.
- Overland, J. E., and M. Wang, 2005: The third Arctic climate pattern: 1930s and early 2000s. *Geophys. Res. Lett.*, **32**, L23808, <https://doi.org/10.1029/2005GL024254>.
- Park, H., E. Watanabe, Y. Kim, I. Polyakov, K. Oshima, X. Zhang, J. S. Kimball, and D. Yang, 2020: Increasing riverine heat influx triggers Arctic Sea ice decline and oceanic and atmospheric warming. *Sci. Adv.*, **6**, eabc4699, <https://doi.org/10.1126/sciadv.abc4699>.
- Park, T.-W., Y. Deng, M. Cai, J.-H. Jeong, and R. Zhou, 2014: A dissection of the surface temperature biases in the Community Earth System Model. *Climate Dyn.*, **43**, 2043–2059, <https://doi.org/10.1007/s00382-013-2029-9>.
- Polyakov, I. V., and Coauthors, 2017: Greater role for Atlantic inflows on sea-ice loss in the Eurasian Basin of the Arctic Ocean. *Science*, **356**, 285–291, <https://doi.org/10.1126/science.aai8204>.
- , A. Pnyushkov, and E. Carmack, 2018: Stability of the Arctic halocline: A new indicator of Arctic climate change. *Environ. Res. Lett.*, **13**, 125008, <https://doi.org/10.1088/1748-9326/aaec1e>.
- , and Coauthors, 2020: Borealization of the Arctic Ocean in response to anomalous advection from sub-Arctic seas. *Front. Mar. Sci.*, **7**, 491, <https://doi.org/10.3389/fmars.2020.00491>.

- Quadrelli, R., and J. M. Wallace, 2004: A simplified linear framework for interpreting patterns of Northern Hemisphere wintertime climate variability. *J. Climate*, **17**, 3728–3744, [https://doi.org/10.1175/1520-0442\(2004\)017<3728:ASLFFI>2.0.CO;2](https://doi.org/10.1175/1520-0442(2004)017<3728:ASLFFI>2.0.CO;2).
- Rehder, Z., A. L. Niederdröck, L. Kaleschke, and L. Kutzbach, 2020: Analyzing links between simulated Laptev Sea sea ice and atmospheric conditions over adjoining landmasses using causal-effect networks. *Cryosphere*, **14**, 4201–4215, <https://doi.org/10.5194/tc-14-4201-2020>.
- Rigor, I. G., J. M. Wallace, and R. L. Colony, 2002: Response of sea ice to the Arctic oscillation. *J. Climate*, **15**, 2648–2663, [https://doi.org/10.1175/1520-0442\(2002\)015<2648:ROSITT>2.0.CO;2](https://doi.org/10.1175/1520-0442(2002)015<2648:ROSITT>2.0.CO;2).
- Rudels, B., 2015: Arctic Ocean circulation, processes and water masses: A description of observations and ideas with focus on the period prior to the International Polar Year 2007–2009. *Prog. Oceanogr.*, **132**, 22–67, <https://doi.org/10.1016/j.pocean.2013.11.006>.
- , E. P. Jones, L. G. Anderson, and G. Kattner, 1994: On the intermediate depth waters of the Arctic Ocean. *The Polar Oceans and Their Role in Shaping the Global Environment. Geophys. Monogr.*, Vol. 85, Amer. Geophys. Union, 33–46, <https://doi.org/10.1029/GM085p0033>.
- , M. Korhonen, U. Schauer, S. Pisarev, B. Rabe, and A. Wisotzki, 2015: Circulation and transformation of Atlantic water in the Eurasian Basin and the contribution of the Fram Strait inflow branch to the Arctic Ocean heat budget. *Prog. Oceanogr.*, **132**, 128–152, <https://doi.org/10.1016/j.pocean.2014.04.003>.
- Sandø, A. B., J. E. Ø. Nilsen, Y. Gao, and K. Lohmann, 2010: Importance of heat transport and local air–sea heat fluxes for Barents Sea climate variability. *J. Geophys. Res.*, **115**, C07013, <https://doi.org/10.1029/2009JC005884>.
- Schauer, U., H. Loeng, B. Rudels, V. K. Ozhigin, and W. Dieck, 2002: Atlantic water flow through the Barents and Kara Seas. *Deep-Sea Res. I*, **49**, 2281–2298, [https://doi.org/10.1016/S0967-0637\(02\)00125-5](https://doi.org/10.1016/S0967-0637(02)00125-5).
- Schlichtholz, P., 2011: Influence of oceanic heat variability on sea ice anomalies in the Nordic seas. *Geophys. Res. Lett.*, **38**, L05705, <https://doi.org/10.1029/2010GL045894>.
- Serreze, M. C., A. D. Crawford, J. C. Stroeve, A. P. Barrett, and R. A. Woodgate, 2016: Variability, trends, and predictability of seasonal sea ice retreat and advance in the Chukchi Sea. *J. Geophys. Res. Oceans*, **121**, 7308–7325, <https://doi.org/10.1002/2016JC011977>.
- , A. P. Barrett, A. D. Crawford, and R. A. Woodgate, 2019: Monthly variability in Bering Strait oceanic volume and heat transports, links to atmospheric circulation and ocean temperature, and implications for sea ice conditions. *J. Geophys. Res. Oceans*, **124**, 9317–9337, <https://doi.org/10.1029/2019JC015422>.
- Shimada, K., T. Kamoshida, M. Itoh, S. Nishino, E. Carmack, F. McLaughlin, S. Zimmermann, and A. Proshutinsky, 2006: Pacific Ocean inflow: Influence on catastrophic reduction of sea ice cover in the Arctic Ocean. *Geophys. Res. Lett.*, **33**, L08605, <https://doi.org/10.1029/2005GL025624>.
- Skagseth, Ø., T. Furevik, R. Ingvaldsen, H. Loeng, K. A. Mork, K. A. Orvik, and V. Ozhigin, 2008: Volume and heat transports to the Arctic Ocean via the Norwegian and Barents Seas. *Arctic–Subarctic Ocean Fluxes: Defining the Role of the Northern Seas in Climate*, R. R. Dickson, J. Meincke, and P. Rhines, Eds., Springer, 45–64.
- Smedsrud, L. H., A. Sirevaag, K. Kloster, A. Sorteberg, and S. Sandven, 2011: Recent wind driven high sea ice area export in the Fram Strait contributes to Arctic sea ice decline. *Cryosphere*, **5**, 821–829, <https://doi.org/10.5194/tc-5-821-2011>.
- , and Coauthors, 2013: The role of the Barents Sea in the Arctic climate system. *Rev. Geophys.*, **51**, 415–449, <https://doi.org/10.1002/rog.20017>.
- Svendsen, L., N. Keenlyside, I. Bethke, Y. Gao, and N.-E. Omrani, 2018: Pacific contribution to the early twentieth-century warming in the Arctic. *Nat. Climate Change*, **8**, 793–797, <https://doi.org/10.1038/s41558-018-0247-1>.
- Swart, N. C., J. C. Fyfe, E. Hawkins, J. E. Kay, and A. Jahn, 2015: Influence of internal variability on Arctic sea-ice trends. *Nat. Climate Change*, **5**, 86–89, <https://doi.org/10.1038/nclimate2483>.
- Thompson, D. W. J., and J. M. Wallace, 1998: The Arctic oscillation signature in the wintertime geopotential height and temperature fields. *Geophys. Res. Lett.*, **25**, 1297–1300, <https://doi.org/10.1029/98GL00950>.
- Vihma, T., 2014: Effects of Arctic Sea ice decline on weather and climate: A review. *Surv. Geophys.*, **35**, 1175–1214, <https://doi.org/10.1007/s10712-014-9284-0>.
- , and Coauthors, 2016: The atmospheric role in the Arctic water cycle: A review on processes, past and future changes, and their impacts. *J. Geophys. Res. Biogeosci.*, **121**, 586–620, <https://doi.org/10.1002/2015JG003132>.
- Wallace, J. M., and D. S. Gutzler, 1981: Teleconnections in the geopotential height field during the Northern Hemisphere winter. *Mon. Wea. Rev.*, **109**, 784–812, [https://doi.org/10.1175/1520-0493\(1981\)109<0784:TITGHF>2.0.CO;2](https://doi.org/10.1175/1520-0493(1981)109<0784:TITGHF>2.0.CO;2).
- Wang, J., and M. Ikeda, 2000: Arctic oscillation and Arctic sea-ice oscillation. *Geophys. Res. Lett.*, **27**, 1287–1290, <https://doi.org/10.1029/1999GL002389>.
- Wang, L., A. Deng, and R. Huang, 2019a: Wintertime internal climate variability over Eurasia in the CESM large ensemble. *Climate Dyn.*, **52**, 6735–6748, <https://doi.org/10.1007/s00382-018-4542-3>.
- Wang, Y., H. Bi, H. Huang, Y. Liu, Y. Liu, X. Liang, M. Fu, and Z. Zhang, 2019b: Satellite-observed trends in the Arctic sea ice concentration for the period 1979–2016. *J. Oceanol. Limnol.*, **37**, 18–37, <https://doi.org/10.1007/s00343-019-7284-0>.
- Warner, J. L., J. A. Screen, and A. A. Scaife, 2020: Links between Barents–Kara Sea ice and the extratropical atmospheric circulation explained by internal variability and tropical forcing. *Geophys. Res. Lett.*, **47**, e2019GL085679, <https://doi.org/10.1029/2019GL085679>.
- Wettstein, J. J., and C. Deser, 2014: Internal variability in projections of twenty-first-century Arctic sea ice loss: Role of the large-scale atmospheric circulation. *J. Climate*, **27**, 527–550, <https://doi.org/10.1175/JCLI-D-12-00839.1>.
- Woodgate, R. A., 2018: Increases in the Pacific inflow to the Arctic from 1990 to 2015, and insights into seasonal trends and driving mechanisms from year-round Bering Strait mooring data. *Prog. Oceanogr.*, **160**, 124–154, <https://doi.org/10.1016/j.pocean.2017.12.007>.
- , T. Weingartner, and R. Lindsay, 2010: The 2007 Bering Strait oceanic heat flux and anomalous Arctic sea-ice retreat. *Geophys. Res. Lett.*, **37**, L01602, <https://doi.org/10.1029/2009GL041621>.
- , —, and —, 2012: Observed increases in Bering Strait oceanic fluxes from the Pacific to the Arctic from 2001 to 2011 and their impacts on the Arctic Ocean water column. *Geophys. Res. Lett.*, **39**, L24603, <https://doi.org/10.1029/2012GL054092>.
- Woods, C., and R. Caballero, 2016: The role of moist intrusions in winter Arctic warming and sea ice decline. *J. Climate*, **29**, 4473–4485, <https://doi.org/10.1175/JCLI-D-15-0773.1>.
- Zhang, R., 2015: Mechanisms for low-frequency variability of summer Arctic sea ice extent. *Proc. Natl. Acad. Sci. USA*, **112**, 4570–4575, <https://doi.org/10.1073/pnas.1422296112>.
- Zhang, X., M. Ikeda, and J. E. Walsh, 2003: Arctic Sea ice and freshwater changes driven by the atmospheric leading mode in a coupled sea ice–ocean model. *J. Climate*, **16**, 2159–2177, <https://doi.org/10.1175/2758.1>.
- Zhong, L., L. Hua, and D. Luo, 2018: Local and external moisture sources for the Arctic warming over the Barents–Kara Seas. *J. Climate*, **31**, 1963–1982, <https://doi.org/10.1175/JCLI-D-17-0203.1>.